

# Balloon-borne Stratospheric Vertical Profiling of Carbonyl Sulfide and Evaluation of Ozone Scrubbing Materials

5 Alessandro Zanchetta<sup>1</sup>, Steven van Heuven<sup>1</sup>, Joram Hooghiem<sup>1,6</sup>, Rigel Kivi<sup>3</sup>, Thomas Laemmel<sup>4</sup>, Michel Ramonet<sup>4</sup>, Markus Leuenberger<sup>5</sup>, Peter Nyfeler<sup>5</sup>, Sophie L. Baartman<sup>6</sup>, Maarten Krol<sup>6,7</sup>, and Huilin Chen<sup>1,2</sup>

<sup>1</sup> Center for Isotope Research (CIO), Energy and Sustainability Research Institute Groningen (ESRIG), University of Groningen, Groningen, the Netherlands

10 <sup>2</sup> Joint International Research Laboratory of Atmospheric and Earth System Sciences, School of Atmospheric Sciences, Nanjing University, Nanjing, China

<sup>3</sup> Space and Earth Observation Centre, Finnish Meteorological Institute (FMI), Sodankylä, Finland

<sup>4</sup> Laboratoire des Sciences du Climat et l'Environnement (LSCE), CEA - CNRS - UVSQ - University Paris-Saclay, Gif sur Yvette, France

15 <sup>5</sup> Climate and environmental Physics, Physics Institute and Oeschger Centre for Climate Change Research, University of Bern, Bern, Switzerland

<sup>6</sup> Meteorology and Air Quality, Wageningen University & Research, Wageningen, the Netherlands

<sup>7</sup> Institute for Marine and Atmospheric Research, Utrecht University, Utrecht, the Netherlands

20 Corresponding to [Huilin.Chen@nju.edu.cn](mailto:Huilin.Chen@nju.edu.cn) or [Huilin.Chen@rug.nl](mailto:Huilin.Chen@rug.nl)

## Abstract

Carbonyl sulfide (COS) is a low abundant atmospheric trace gas that has a tropospheric lifetime of 2-2.5 years, allowing it to reach the stratosphere, where it undergoes photolysis and reactions with OH• and O• radicals, generating precursors of stratospheric aerosols. Vertical profiling of COS has rarely been realised, especially for stratospheric observations. In this study, we introduce a new technique for continuous and discrete vertical profiling of COS based on the analysis of air samples collected by AirCore, the LIghtweight Stratospheric Air (LISA) sampler and its scaled-up version BigLISA in three campaigns in Trainou (2019), Kiruna (2021) and Sodankylä (2023) using a Quantum Cascade Laser Spectrometer (QCLS). To eliminate potential COS measurement biases, we have investigated the efficiency of different scrubbers based on cotton and squalene for removing ozone (O<sub>3</sub>) and assessed their potential impacts on COS measurement. Furthermore, we examined the influence of different inlet configurations and O<sub>3</sub> scrubbers on the retrieved COS profiles, and found no significant impact within the uncertainties. We found that the differences with the averaged profiles obtained from the Atmospheric Chemistry Experiment – Fourier Transform Spectrometer (ACE-FTS) and the measured AirCore profiles at both mid and polar latitudes were less than 5%, and approximately 10% for the LISA samples at polar latitudes. Differences between our observations and COS observations from the *SPectromètre InfraRouge d'Absorption à Lasers Embarqués* (SPIRALE) ranged from 10% to 15%, with

35

both methods showing similar COS trends over altitude. Moreover, we found squalene-based scrubbers to be suitable for quantitative O<sub>3</sub> removal. Both AirCore and the LISA samplers are lightweight and suitable for routine balloon-borne COS profiling, providing useful observations for stratospheric research and validation of COS retrievals from remote sensing techniques.

## 40 1. Introduction

Carbonyl sulfide (COS, also referred to as OCS) is an odorless and colorless gas species (Ferm, 1957). It is the most abundant sulfur-containing gas species in the atmosphere, with a tropospheric mole fraction of 350-500 parts per trillion (ppt, pmol/mol) in the unpolluted free troposphere (Berry et al., 2013; Remaud et al., 2023). It has been suggested as a proxy to partition photosynthetic uptake of CO<sub>2</sub> from respiration, to improve the quantification of carbon fluxes between atmosphere and  
45 vegetation (Campbell et al., 2008; Montzka et al., 2007; Sandoval-Soto et al., 2005; Stimler et al., 2009; Whelan et al., 2018). Given its relatively long tropospheric lifetime of 2-2.5 years (Ma et al., 2021; Montzka et al., 2007; Remaud et al., 2023), COS can reach the stratosphere, where it is converted to CO<sub>2</sub> and sulfur dioxide (SO<sub>2</sub>), a precursor of stratospheric aerosols, by photolysis and reactions with OH• and O• radicals (Brühl et al., 2012; Chin and Davis, 1995; Krysztofiak et al., 2015). COS is considered to likely be the largest contributor to stratospheric sulfur aerosols during volcanic quiescent periods (Brühl et al.,  
50 2012; Crutzen, 1976; Kremser et al., 2016).

Currently, observations of stratospheric COS vertical profiles and/or total columns are performed by ground- and satellite-based remote sensing (Barkley et al., 2008; Bernath, 2005; Toon et al., 2018) and by deploying balloon-borne spectrometers (Krysztofiak et al., 2015; Toon et al., 2018). The collection of air samples for COS analysis was only carried out sporadically  
55 or only in the upper troposphere/lowermost stratosphere (10-12 km) (Engel and Schmidt, 1994; Karu et al., 2023). In this paper, we present new techniques to collect continuous and discrete stratospheric air samples, based on the balloon-borne AirCore (Karion et al., 2010) and the Lightweight Stratospheric Air (LISA) (Hooghiem et al., 2018) and BigLISA samplers, respectively, paired with a Quantum-Cascade Laser Spectrometer (QCLS, Aerodyne Research Inc., MA, USA, model TILDAS-CS) for COS measurements (Kooijmans et al., 2016; Stimler et al., 2009). These methods allow analysis of collected  
60 air samples with minimal preparation and treatment, which reduces risks of contamination during sampling and storage.

Possible impacts of stratospheric ozone (O<sub>3</sub>) (Engel and Schmidt, 1994) as well as pollution-induced tropospheric O<sub>3</sub> (Andreae et al., 1990, 1993; Hofmann et al., 1992; Persson and Leck, 1994) on collected air samples for COS observations have been reported in previous studies. O<sub>3</sub>, a strong oxidant, may in fact react with reduced sulfur compounds causing a variable, yet  
65 possibly significant reduction in their abundance (Andreae et al., 1990; Engel and Schmidt, 1994; Hofmann et al., 1992; Persson and Leck, 1994). Since stratospheric O<sub>3</sub> is more abundant than pollution-induced tropospheric O<sub>3</sub> (in particular between 15 and 35 km of altitude, where O<sub>3</sub> mixing ratios may reach roughly 10 ppm) (World Meteorological Organization

(WMO), 1999), its impact on air samples for COS observations may be significant. Therefore, we have investigated different techniques to remove O<sub>3</sub> before sampling, and assessed their potential impacts on the mole fractions of COS and other trace gases. In particular, we have investigated different O<sub>3</sub> scrubbers and their scrubbing efficacy and effect on COS, also by deploying different inlets on the aforementioned samplers. Furthermore, we show a comparison of measured continuous and discrete COS samples with previous observations. A particular focus is set on a cross-validation comparison with SPIRALE's in situ spectrometry (Krysztofiak et al., 2015) and ACE-FTS remote sensing COS observations (Bernath, 2005; Glatthor et al., 2017; Schmidt et al., 2024; Velazco et al., 2011).

## 75 2. Materials and methods

### 2.1 Samplers

The three different samplers deployed to collect stratospheric air will be presented in this section. All instruments flew under weather balloons that typically reached altitudes of 30 to 35 km. The presented data was collected in different campaigns, namely the RINGO campaign in Trainou (TRN, France, 2019), the HEMERA campaign (Schuck et al., 2025) in Kiruna (KRN, Sweden, 2021) and the OSTRICH campaign at the Fourier Transform Spectrometer (FTS) site (Kivi and Heikkinen, 2016) in Sodankylä (SOD, Finland, 2023). An overview of campaigns and samplers is reported in Table 1. Air samples collected by all devices were analysed on a QCLS, which will be described in Sect. 2.2.

#### 2.1.1 AirCore

The AirCore sampler was first introduced by Karion et al. (2010) to retrieve CO<sub>2</sub> and CH<sub>4</sub> vertical profiles. It consists of a long, stainless-steel tube usually shaped as a coil, internally coated with Sulfinert® to prevent reactions or adsorption of gas species with the tube walls (Karion et al., 2010; Membrive et al., 2017). When used to retrieve vertical profiles, AirCore sampling is realised passively and continuously along the coil at ambient temperature (Karion et al., 2010; Membrive et al., 2017; Wagenhäuser et al., 2021), differently from the discrete samples that can be collected by cryosamplers which, however, need to be cooled down to 27 K with liquid neon before flight (Laube et al., 2010; Schmidt et al., 1987). Before the flight, the coil is filled with a known gas mixture, which will later help identifying the starting point of the AirCore profiles during analysis. During ascent, the coil empties through one open end due to decreasing ambient pressure. After the balloon bursts, the instrument collects air during descent while ambient pressure is increasing, without using a pump. Knowing sampling pressure and temperature, and assuming pressure equilibrium during the filling process, each aliquot of moles of air can be calculated for each sampling altitude interval. These can be associated to the aliquot of analysed moles of air in the coil, allowing the retrieval of vertical profiles (Karion et al., 2010; Membrive et al., 2017; Tans, 2022). However, the selected start and end point of each analysis, air mixing inside the coil, sample loss, and general fill dynamics may all be causes for deviations from this approximation (Membrive et al., 2017; Tans, 2022; Wagenhäuser et al., 2021). Detailed discussions of fill dynamics and uncertainties treatment can be found in Tans (2022) and Membrive et al. (2017), respectively. In this study, we followed

the approach described by Membrive et al. (2017) to retrieve the altitude mapping and the relative uncertainties along the vertical profiles, with one exception, as follows.

As reported in Table 1, flight SOD3 included a double-sided sampling AirCore, property of the University of Bern, which was flown and analysed by our group. One half of this 200 m long AirCore was equipped with an oxygen-spiking system, programmed to inject 5 minuscule shots of O<sub>2</sub> in the coil as altitude markers at 21045, 17005, 11837, 7870 and 4592 m. Although our QCLS is not capable of measuring O<sub>2</sub>, these injections were visible as COS anomalies along the profile (see Sect. 4.1). Therefore, the altitude mapping for this AirCore was realised by matching the COS spikes with the reported spiking altitudes. Moreover, the cotton scrubber installed on one of the two inlets likely adsorbed water (H<sub>2</sub>O) before the ascent phase, which was then taken in the AirCore at the beginning of the descent, mixing tropospheric H<sub>2</sub>O with stratospheric air at the highest altitude. This required a dilution correction, followed by a matrix effect correction inferred from the correlation of different species with H<sub>2</sub>O mole fraction.

At the altitude ceiling of the balloon flight, the AirCore's coil still contains part of the fill gas. This remaining fill gas can mix with the sampled air at the top of the profile. Similarly, air from the lowest part of the sampled profile mix with the gas used to push the air out of the coil during analysis. Therefore, the highest and the lowest parts of the profiles are flagged and are not used for further analysis.

For the double-sided AirCore deployed on flight SOD3, fill gas flagging starts at lower altitude compared to other AirCores. Given the design of this AirCore, air is collected from both ends of the coil, allowing the simultaneous sampling of two profiles. Therefore, the top of the profiles and the remaining fill gas are located at the centre of the coil and not at one of its ends. For all other AirCores, the top of the profile is the first part to be analysed, while for this sampler it will have to travel 100 m through the coil before reaching the analyser. Thus, during analysis the top of the profile and the remaining fill gas have a longer time to get mixed compared to other AirCores. Moreover, the resulting gas mixture may also experience a stronger smearing effect due to its path through the coil. Altogether, this determines a larger portion of the profile that cannot be considered for analysis compared to other AirCores.

Some AirCores experienced COS contamination due to specific design features (e.g., differential pressure sensors along the coil or glue connections). Consequently, the contaminated COS mole fractions have been removed and are shown as gaps. The causes of contamination are discussed in Sect. 4.1.

### 2.1.2 LISA sampler

The LISA sampler used in this study is a further miniaturised (55 L package size) and light-weight (2.9 kg) version of the original sampler developed by Hooghiem et al. (2018). The instrument is battery-powered and is controlled by a microcontroller, which also logs GPS, pressures, temperatures, and general instrument status. Differently from AirCore, LISA

actively pumps ambient air into four different 2.5L multi-layer foil (MLF) bags (type 30228-U, Supelco Inc., USA) through a custom-made manifold. The sampling is performed during the ascent phase of the flight, since the vertical speed is slower than during descent and this allows for a higher vertical resolution of the vertical sampling. The valves of the MLF bags are opened and closed by servos. The sampling pressure intervals for each bag are programmed before the flight and limited to an absolute pressure of 280 hPa to prevent bag burst after sampling. This is necessary because the ambient pressure continues to decrease during the remainder of the ascent, reaching about 10 hPa at 30 km altitude. The sampling pressures and the derived sampling altitude intervals and sample volumes are reported in Table S1 in the Supplement. The mid-points of sample collections are calculated considering the dependency of pump performance on the ambient pressure and the bag filling status, as described by Hooghiem et al. (2018).

Unusually high COS mole fractions were measured in laboratory tests and in some collected samples, which we speculate being due to outgassing from polymers (Lee and Brimblecombe, 2016). Therefore, during the SOD campaign in 2023, we performed pre-conditioning of the MLF bags differently from what Hooghiem et al. (2018) described. Before each flight, MLF bags were not only filled and vacuumed with purified N<sub>2</sub>, but filled and vacuumed repeatedly with air from a cylinder of synthetic air mixed with low mole fractions of CH<sub>4</sub>, CO<sub>2</sub> and CO, which was meant to simulate stratospheric air conditions and contained 0 ppb N<sub>2</sub>O and 0 ppt COS. This was done to prevent outgassing of different gas species, and in particular COS, from the polymers composing the MLF bags. The gas mixture used to flush the bags was measured on the QCLS before filling the bags and when it was pumped out from them, allowing a control of potential contaminations under stratospheric sampling conditions. After the LISA sampler was recovered and brought back to the laboratory in the field, LISA air samples were transferred to glass flasks and stored for later analyses of COS and other trace gas species. Here we present the analysis results of the air samples left in the sampling bags, when present, directly after the sample transfer from the MLF bags to glass flasks (these latter were not analysed on the QCLS). The leftover volume of one of these samples was insufficient for analysis (SOD3 – L4), while two others showed unusually high mole fractions for several of the analysed gas species (SOD2 – L4, SOD5 – L3), in spite of the pre-conditioning of these bags before flight. These three samples were labelled as outliers and will not be presented in this work.

### 2.1.3 BigLISA

BigLISA is a larger-volume and functionally improved variant of the LISA sampler, with a mass of roughly 12 kg. On the HEMERA missions in KRN, two independently operating BigLISA samplers were flown in a single enclosure on a high-payload balloon (Schuck et al., 2025). Each BigLISA unit consists of a central box containing electronics and pneumatic components, and 6 externally mounted 10 L MLF bags (type 30229-U, Supelco Inc., USA). The BigLISA pneumatic hardware consists of a two-stage pump, a flow-reversing valve system that allows purging, a manifold and 6 closable MLF bags, all powered, monitored and controlled from a single control board.

165 Two stage-pumping is attained by connecting the four heads of two double-headed pumps (model NMP830.1.2KPDC-B HP, KNF, Germany) in a three to one configuration. This attains a high flow rate and a high compression factor. Laboratory tests confirmed the potential to reach a compression ratio of 25 at low ambient pressures. However, potentially due to unfavourably dimensioned connecting tubing, the compression ratio obtained during flight ranged between 2 and 5 times over ambient pressure.

170

Operation and logging are provided by a custom-made Printed Circuit Board (PCB) running an ESP32 microcontroller (Adafruit Industries, model HUZZAH32). Temperature is monitored at the pump heads, battery packs, power converters and within the larger BigLISA outer housing. In each pack, before and between pumping operations, the two 3-way valves are actuated as necessary to maintain in-pack temperature above 5 °C, preventing loss of battery capacity and conceivable pump stalling. Power for electronics, pumps and valves is provided by two packs (for redundancy) of eight Saft LSH14 Li-SOCl<sub>2</sub> cells.

175 Housing for the two BigLISA units was provided by a customised high strength but lightweight aluminium frame, that was able to withstand the high accelerations potentially experienced during parachute deployment. In this structure, the two BigLISA packs are mounted centrally, surrounded by the 6 + 6 MLF bags, that are individually suspended using tie-wraps on concentric stainless-steel wires. Protection from wind and radiation is provided by 1 mm thick aluminium sheeting. GPS receivers and sampling inlet pumping lines are led out radially at the top of the package.

180 During ascent, starting at 120 hPa (~15 km), bags were (re-)evacuated by the two-stage pump. This procedure removes conceivable traces of tropospheric air from the bags, and tests for plumbing integrity. From 30 hPa (~25 km), the manifold was flushed with ambient air to clear it of residual tropospheric air and water vapour. Just prior to collecting a sample, the respective bag would be repeatedly filled with a tiny amount of air and evacuated, to dilute away any residual air in it. Sampling took place during the descent, for as long as it took to reach 200 hPa of sample pressure, but never more than 1800 seconds (less for lower samples), and would stop when the next sample was due to be collected. The sampling altitude intervals are reported in Table S1 in the Supplement and are shown in Figure 1. The mid-points of sampling altitudes were calculated similarly to Hooghiem et al. (2018), considering the decreased pump performance when compression become necessary to fill the bag. However, given that BigLISA sampled during descent, this effect was counteracted by the increase in ambient pressure during sampling. Therefore, the mid-points of BigLISA fall more towards the average of the sampling interval than the ones of LISA. Similarly to LISA, samples labelled as outliers due to unusually high mole fractions of multiple tracers (KRN - BL7, BL10, BL11 and BL12) will not be presented in this text.

185

190

195 **Table 1: overview of the instruments deployed for COS sampling, the launch location, samplers' sizes and additional features, and the inlet features in different campaigns. The reported diameters ( $\emptyset$ ) refer to the outer diameter of the tubing. The flight code helps identifying which instruments have been deployed on the same balloons, and is used to refer to these flights in the text.**

<b>Location</b>	<b>Flight code</b>	<b>Flight date and takeoff time (UTC)</b>	<b>Apogee</b>	<b>Instrument</b>	<b>Instrument features</b>	<b>Inlet features</b>
Trainou (FRA) 47°58' N 2°06' E	TRN1	17/06/2019 12:30	34.6 km	AirCore	23 m x $\emptyset$ 8 mm + 46 m x $\emptyset$ 4 mm V ~ 1600 cm <sup>3</sup>	Free inlet
	TRN2	18/06/2019 8:00	32.6 km	AirCore	36 m x $\emptyset$ 3/16" + 38 m x $\emptyset$ 1/8" V ~ 830 cm <sup>3</sup>	Mg(ClO <sub>4</sub> ) <sub>2</sub> dryer
	TRN3	18/06/2019 10:39	34.9 km	AirCore	23 m x $\emptyset$ 8 mm + 46 m x $\emptyset$ 4 mm V ~ 1600 cm <sup>3</sup>	Free inlet
	TRN4	20/06/2019 07:07	32.3 km	AirCore	36 m x $\emptyset$ 3/16" + 38 m x $\emptyset$ 1/8" V ~ 830 cm <sup>3</sup>	Free inlet
Kiruna (SWE) 67°53' N 21°04' E	KRN	12/08/2021 21:18	33.1 km	AirCore	37 m x $\emptyset$ 3/16" + 39 m x $\emptyset$ 1/8" V ~ 860cm <sup>3</sup>	Mg(ClO <sub>4</sub> ) <sub>2</sub> dryer
	KRN	12/08/2021 21:18	33.1 km	AirCore	36 m x $\emptyset$ 3/16" + 38 m x $\emptyset$ 1/8" V ~ 830 cm <sup>3</sup>	Free inlet
	KRN	12/08/2021 21:18	33.1 km	BigLISA	12 x 10 L MLF-bags	Mg(ClO <sub>4</sub> ) <sub>2</sub> dryer
Sodankylä (FIN) 67°22' N 26°37' E	SOD1	02/08/2023 7:00	29.7 km	AirCore	40 m x $\emptyset$ 1/4" + 58 m x $\emptyset$ 1/8" V ~ 1400 cm <sup>3</sup> Differential pressure sensors	Mg(ClO <sub>4</sub> ) <sub>2</sub> dryer

	SOD2	02/08/2023 14:50	30.1 km	LISA	4 x 2.5 L MLF- bags, pre- conditioned	Mg(ClO <sub>4</sub> ) <sub>2</sub> dryer
	SOD3	05/08/2023 10:56	26.3 km	LISA	4 x 2.5 L MLF- bags, pre- conditioned	Free inlet
	SOD3	05/08/2023 10:56	26.3 km	AirCore	200 m x Ø 1.5 mm” V ~ 1400 cm <sup>3</sup> Double-sided sampling	One side free inlet, one side cotton-based O <sub>3</sub> scrubber
	SOD4	06/08/2023 9:03	29.8 km	LISA	4 x 2.5 L MLF- bags, pre- conditioned	Cotton- based O <sub>3</sub> scrubber
	SOD5	08/08/2023 6:17	29.3 km	AirCore	40 m x Ø 1/4” + 58 m x Ø 1/8” V ~ 1400 cm <sup>3</sup> Differential pressure sensors	Mg(ClO <sub>4</sub> ) <sub>2</sub> dryer and cotton-based O <sub>3</sub> scrubber

## 2.2 Quantum Cascade Laser Spectrometer (QCLS)

The trace gas analyser used to perform COS measurements in all campaigns is a dual laser QCLS by Aerodyne Research Inc. (Billerica, MA, USA), operating in the mid-infrared frequencies. This technique was firstly introduced for COS measurements by Stimler et al. (2009) and further developed by Kooijmans et al. (2016). The QCLS employed in this study has also been used in previous UAV- and aircraft-borne tropospheric active AirCore measurements for CH<sub>4</sub> and N<sub>2</sub>O (Tong et al., 2023; Vinković et al., 2022), as well as in situ tropospheric COS observations (Zanchetta et al., 2023). The QCLS can measure CH<sub>4</sub>, CO<sub>2</sub>, N<sub>2</sub>O, CO, COS, H<sub>2</sub>O, and O<sub>3</sub> simultaneously. Its cavity is controlled at a temperature of 298 K and a pressure of ~66 hPa (50 Torr). The QCLS measures at a constant mass flow of 50 mL min<sup>-1</sup> and the measured data is output at 1 Hz. For COS, the precision (1σ) falls usually between 15 and 25 ppt at 1 Hz, depending on the laboratory conditions (e.g., ambient temperature stability). The cell of the QCLS has a volume of 150 mL, which at 50 Torr corresponds to an effective cavity volume of ~10 mL. The spatial resolution of AirCore measurements in this configuration is roughly 2000 m at 28 km, 300 m at 15 km and 200 m at 10 km altitude, which resembles the resolution ranges presented by Membrive et al. (2017). The QCLS is controlled with a custom-made frontend, operated via a dedicated software, which allows switching between different inlets without causing changes in pressure through the system. Overall, the instrument achieves a precision better than 0.6 ppb for CH<sub>4</sub>, 0.2 ppm for CO<sub>2</sub>, 0.12 ppb for N<sub>2</sub>O, 1 ppb for CO, 20 ppt for COS, 20 ppm for H<sub>2</sub>O, and 100 ppb for O<sub>3</sub>.

As reported in Zanchetta et al. (2023), field standard cylinders are calibrated against NOAA standards (NOAA-2004 COS scale) in the laboratory before and after each measurement period to test for drift in the molar fraction of gas species. The COS mole fraction measurements of nine cylinders are available, and five cylinders changed by less than 2.5 ppt yr<sup>-1</sup>, two cylinders decreased by ~ 10 ppt yr<sup>-1</sup> and two cylinders decreased by ~ 30 ppt yr<sup>-1</sup>. The four cylinders that drifted more than 10 ppt yr<sup>-1</sup> were not used as reference cylinders in the data processing. All of the cylinders were uncoated aluminium cylinders, which, according to experience at NOAA, are more prone to COS mole fraction drift than Aculife-treated aluminium cylinders. More details on the instrumental calibration, precision and stability can be found in Kooijmans et al. (2016).

## 220 **2.3 Datasets for COS profiles comparison and validation**

For validation purposes, our COS profiles were compared to the SPIRALE results reported by Krysztofiak et al. (2015), as well as a selection from the Atmospheric Chemistry Experiment – Fourier Transform Spectrometer (ACE-FTS, v5.3) dataset (Bernath, 2005; Boone et al., 2023; Schmidt et al., 2024; Velazco et al., 2011).

### **2.3.1 SPIRALE**

225 The in situ balloon-borne SPIRALE spectrometer presented by Krysztofiak et al. (2015) was deployed in two flights at polar latitudes (Kiruna, Sweden, 67°53' N 21°04' E) in 2009 and 2011. The resulting COS profiles cover altitudes between 14.3 – 21.6 km and 18.5 – 22.0 km, respectively. Given the different altitudinal resolution, both the measured AirCore profiles and the SPIRALE results were averaged in 0.5 km bins to calculate the difference between COS mole fractions. A comparison between AirCore and SPIRALE COS profiles is shown in Figure 3.

### 230 **2.3.2 ACE-FTS**

ACE-FTS is a satellite-borne spectrometer measuring altitude profile information for temperature, pressure, and mole fractions of several gas species (Bernath, 2005; Glatthor et al., 2017; Velazco et al., 2011), including COS, by sun occultation. Each profile of ACE-FTS contains 1 km resolution data from 0-150 km altitude. To have a comparable dataset with the measured AirCore profiles, COS ACE-FTS observations realised between June and September in the 2012 – 2024 period were selected, with latitudes ranging between 45-49° N for TRN and 65-69° N for KRN and SOD, resulting in 502 and 1681 COS profiles, respectively. These selected profiles were then averaged for both latitudinal ranges. The COS profiles measured with AirCore in this study are averaged over 1 km intervals to obtain a comparable dataset. The resulting averaged profiles and their comparison with the observed AirCore profiles are shown in Figure 7.

### 3. Results

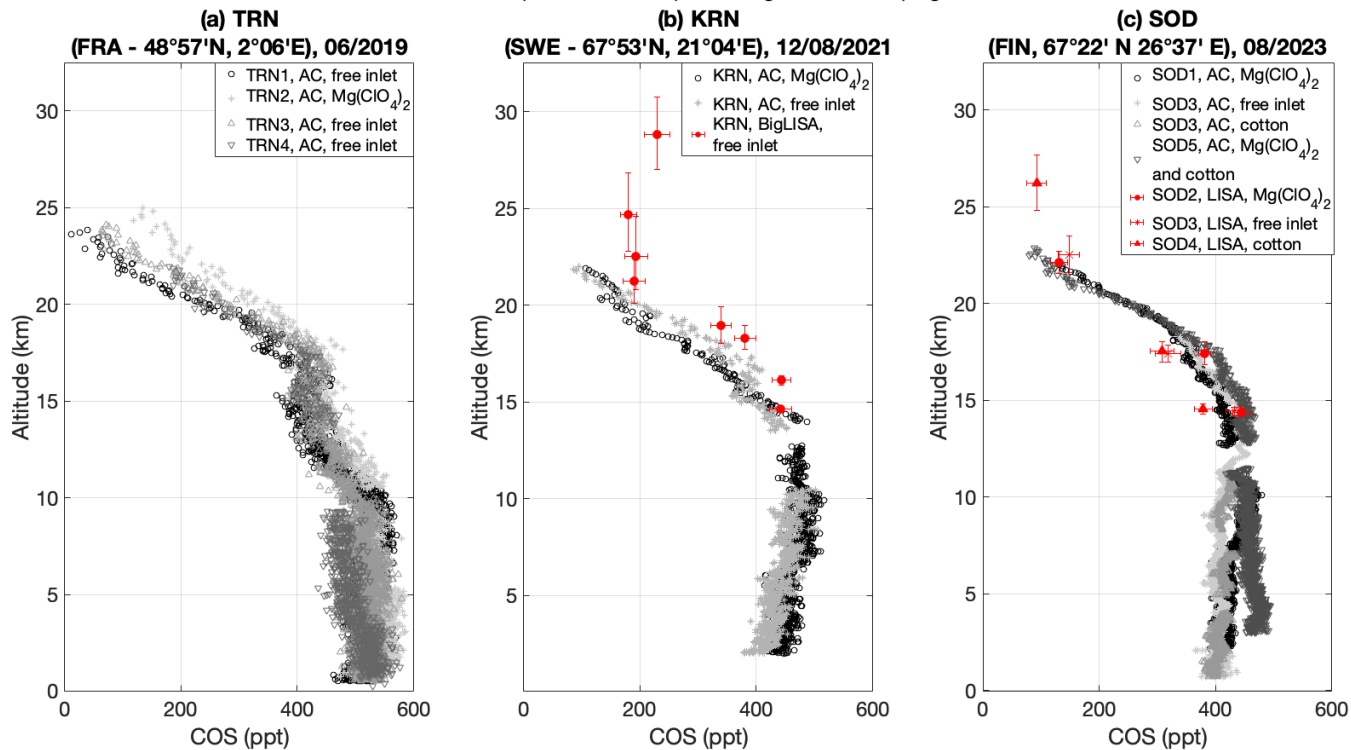
#### 240 3.1 COS observations

Figure 1 shows the COS profiles measured from AirCores and the LISA/BigLISA samples of the campaigns reported in Table 1. For all campaigns, different inlets were deployed. Different inlet configurations are reported in Table 1 and in the figure captions.

245 The tropospheric COS mole fractions vary from flight to flight, ranging between about 400 to 500 ppt. The thermal tropopause height (World Meteorological Organization, 1957) was between about 10.6 and 11.5 km at mid latitudes (TRN, June 2019, Fig. 1a), and between 9.9 and 10.9 km at polar latitudes (KRN, August 2021, Fig. 1b and SOD, 2023, Fig. 1c), respectively (see Fig. S7-S15 in Sect. S4 of the supplement). The COS stratospheric sink is clearly noticeable for all campaigns above the tropopause and is further discussed in Sect. 4.1. At polar latitudes, the COS mole fraction decreases from an all-campaigns  
250 average of  $421 \pm 26$  ppt below 17 km to  $180 \pm 15$  ppt between 20 and 22 km. At mid-latitudes, the mole fractions decrease from a campaign average of  $488 \pm 12$  ppt below 17 km to  $220 \pm 59$  ppt between 20 and 22 km.

As reported in Table 2, the BigLISA samples measured in KRN in 2021 show consistently higher mole fractions when compared to the AirCore profiles. By contrast, the LISA samples measured in SOD in general show good agreement with the  
255 continuous profiles. The largest difference was found in SOD3, between a collection of free-inlet LISA samples and an AirCore equipped with a cotton scrubber obtained from the same flight. The possible explanations for these differences are discussed in Sect. 4.1.2.

Measured COS profiles and samples during different campaigns



260 **Figure 1:** measured COS AirCore (AC) profiles and LISA/BigLISA samples in different sampling campaigns.

**Table 2:** COS mole fraction difference between AirCore and (Big)LISA samples that flew on the same days. The AirCore COS mole fraction is calculated as the COS average over (Big)LISA's sampling altitude range.

(Big)LISA sample name	Altitude range (km)	$\Delta$ COS (ppt) AirCore – (Big)LISA	Inlets features	Average $\Delta$ COS (ppt)
KRN – BL3	20.1 – 22.5	-48	AirCore: Mg(ClO <sub>4</sub> ) <sub>2</sub> dryer BigLISA: Mg(ClO <sub>4</sub> ) <sub>2</sub> dryer	$-80 \pm 50$
KRN – BL9	18.0 – 19.9	-125		
KRN – BL4	17.7 – 19.0	-133		
KRN – BL5	15.9 – 16.4	-78		
KRN – BL6	14.5 – 14.7	-16		
KRN – BL3	20.1 – 22.5	-52	AirCore: free inlet BigLISA: Mg(ClO <sub>4</sub> ) <sub>2</sub> dryer	$-53 \pm 20$
KRN – BL9	18.0 – 19.9	-68		
KRN – BL4	17.7 – 19.0	-70		
KRN – BL5	15.9 – 16.4	-53		
KRN – BL6	14.5 – 14.7	-21		

SOD1 – L1	14.1 – 14.6	-32	AirCore: Mg(ClO <sub>4</sub> ) <sub>2</sub> dryer LISA: Mg(ClO <sub>4</sub> ) <sub>2</sub> dryer	-16 ± 24
SOD1 – L2	16.8 – 18.0	-27		
SOD1 – L3	21.5 – 22.7	11		
SOD3 – L1	14.2 – 14.6	17	AirCore: free inlet LISA: free inlet	31 ± 20
SOD3 – L2	17.0 – 17.9	46		
SOD3 – L3	21.6 – 23.5	No AirCore data		
SOD3 – L1	14.2 – 14.6	25	AirCore: cotton, without dryer LISA: free inlet	/
SOD3 – L2	17.0 – 17.9	No AirCore data		
SOD3 – L3	21.6 – 23.5	No AirCore data		

## 4. Discussion

### 265 4.1 Collected COS profiles and (Big)LISA samples

#### 4.1.1 COS profiles

The AirCore data presented in Figure 1 show continuously sampled stratospheric COS profiles collected with balloon-borne instruments. Previous stratospheric or Upper Troposphere/Lowermost Stratosphere (UT/LMS) observations were realised with discrete whole-air sampling (Engel and Schmidt, 1994; Karu et al., 2023), in situ spectrometers (Gurganus et al., 2024 (preprint); Kloss et al., 2021; Krysztofiak et al., 2015; Leung et al., 2002; Wofsy et al., 2017; Wofsy, 2011) or remote sensing (Glatthor et al., 2017; Toon et al., 2018; Velazco et al., 2011; Yousefi et al., 2019). LISA and BigLISA represent lightweight additions to these methods. For validation purposes, AirCore, LISA and BigLISA observations have been compared with SPIRALE in situ observation (Krysztofiak et al., 2015) and the ACE-FTS remote sensing observations (Bernath, 2005; Velazco et al., 2011).

275

The occasional data gaps shown in the AirCore profiles have different reasons, as summarised in Table 3. TRN4 and the KRN AirCore equipped with Mg(ClO<sub>4</sub>)<sub>2</sub> had tubing of two different diameters, which were connected to each other using a sleeve adapter into which they were glued using Loctite Super Attak glue. SOD1 and SOD5 AirCores, instead, were equipped with differential pressure sensors (Amsys, model AMS5915\_0050\_D\_B) and showed signs of COS contamination at the sensors' location. SOD3 AirCore showed COS spikes related to the O<sub>2</sub> altitude-mapping technique employed in one of its halves. COS outgassing from sulfur-containing polymers, in particular rubbers, has been reported in several studies (Cadle and Williams, 1978; Levine et al., 2023; Pos and Berresheim, 1993). We speculate that the polymers constituting the glue, or components of valves (e.g., O-rings) and differential pressure sensors, may have caused the COS outgassing. In the case of SOD3, another possibility could be direct oxidation reactions of reduced sulfur gas species with O<sub>2</sub>.

280

Nonetheless, the AirCore profiles we presented are similar to observations reported by previous studies: in TRN, COS mole fraction first decreases from tropospheric values of about 510 ppt up to around 10.5 km, to about 420 ppt at 17 km. Then, it undergoes a faster decrease to 92 – 203 ppt at 22 km. This is consistent with observations reported in previous studies at comparable latitudes (Leung et al., 2002; Toon et al., 2018). Although altitude itself does not provide a precise proxy for quantitative comparisons of vertical profiles, this agreement is a strong suggestion of robust stratospheric COS measurements.

At polar latitudes, we observed larger tropospheric variability. The profiles showed tropospheric COS mole fractions ranges between 400 – 470 ppt. Glatthor et al. (2017) reported values at 5 km altitude as low as 330 ppt for COS, during northern summer months at polar latitudes between 2003 – 2012, while Toon et al. (2018) showed a value around 410 ppt under similar conditions. Regarding the stratospheric part of the profile, we observed slight increases or stable values up to 13 – 15 km range (350 – 450 ppt), followed by decreases down to 95 – 130 ppt around 22 km. Most flights from the SOD campaign, in particular SOD1 and SOD5, were characterised by variable lapse rates above the tropopause (see Sect. S4 in the Supplement) which we suspect may be an indicator for COS convective transport and mixing in the lowermost stratosphere. Nevertheless, the observed stratospheric COS range seems consistent with previous studies. Leung et al. (2002) reported 440 ppt below 14 km, decreasing to 120 ppt at 22 km. Glatthor et al. (2017) reports around 490 ppt at 13 km, followed by a decrease to 140 ppt at 22 km. Kryzstofiak et al. (2015) reported  $420 \pm 100$  ppt COS below 17 km, decreasing to 150 ppt at 22 km. A more quantitative comparison between our profiles and Kryzstofiak et al. (2015) and ACE-FTS (Bernath, 2005; Velazco et al., 2011; Yousefi et al., 2019) observations is presented in Sect. 4.2 and 4.3, respectively.

#### 4.1.2 (Big)LISA samples

The samples from KRN BigLISA show clear signs of contamination, in particular above 20 km (Figure 1). We believe this may be due to COS outgassing from some plastic components of the MLF bags used to collect the samples, such as the O-ring in the valves, or simply tropospheric air that remained trapped inside the bag. Although all the deployed bags are indicated as suitable for sulfur compounds, they are not recommended for low-ppm volatile organic compounds due to background levels (Sigma Aldrich, 2025). This might have also influenced our COS measurements, perhaps due to spectroscopic effects. The contamination appears to be inversely proportional to the sampling pressure and the collected sample volume. Unfortunately, it has not been possible to assess the cause of this contamination precisely. Given these circumstances and the impossibility of applying any correction to these results, BigLISA will be left out of the discussion and comparisons with other datasets.

However, as described in Sect. 2.1.2, during the SOD campaign we introduced a pre-treatment technique that has mitigated this issue for COS, based on previous laboratory tests. Filling and vacuuming the bags with a stratospheric-mimicking gas seemed to have reduced the contamination significantly for most LISA samples, as previously reported in Figure 1 and Table 2. However, in some cases and in particular for smaller samples collected at higher altitudes (SOD2 – L4, SOD5 – L3), this

pre-conditioning was not sufficient to prevent biases that are likely ascribable to the bags employed during the campaign. For the remaining samples, when LISA flew on the same balloon as one of our AirCores (e.g. SOD1, SOD3), the largest average difference of  $31 \pm 15$  ppt was found when both instruments were flown with a free inlet. Although some variability can be observed between different LISA samples at similar altitudes, their COS mole fraction falls well within the range of the AirCore profiles (see Sect. 4.1.3, 4.2 and 4.3).

### 4.1.3 Datasets consistency

Figure 2 shows the measured COS AirCore profiles and LISA samples from all campaigns, plotted against altitude above tropopause (see Sect. S4 in the Supplement). TRN1 is not presented in this figure, since the tropopause height could not be estimated due to missing temperature and relative humidity. Differences of up to  $\sim 100$  ppt can be clearly seen between the measured profiles. However, these differences are not constant with altitude and do not show any clear trend over the time span of the campaigns. Moreover, these differences do not show any clear relationship with the different inlets employed.

The most likely explanation for differences between the measured profiles may reside in stratospheric horizontal transport from different latitudes (Toon et al., 2018). The tight correlation between  $\text{CH}_4$  and  $\text{N}_2\text{O}$  (Sect. S5 in the Supplement) suggests that the day-to-day variability can likely be ascribed to atmospheric transport (Kondo et al., 1996; Plumb, 2007; Plumb and Ko, 1992). Moreover, long-term changes in COS seasonal cycle, sources and sinks (Belviso et al., 2022; Schmidt et al., 2024; Sturges et al., 2001) may affect its stratospheric abundance, although no significant stratospheric trends have been observed in the last decades (Barkley et al., 2008; Coffey and Hannigan, 2010; Rinsland et al., 2008; Toon et al., 2018).

Other possible causes of the differences between the profiles may reside in a combination of instrumental uncertainties, altitude mapping algorithms, sample loss after landing, contaminations and instrumental features (e.g., inlets, different air mixing in the AirCore coil during sampling). Overall, it is difficult to assess the contribution of each of these parameters quantitatively. Instrumental uncertainties and altitude mapping are consistent for our results. No quantification of sample loss is available, but given the AirCore design, this should mostly affect the tropospheric part of the profiles. Some clear contaminations affecting AirCore profiles (Table 3) and (Big)LISA samples were marked as outliers, but it is still possible that more subtle effects affected the samples. These may include mixing with dead volumes of tropospheric air or fill gas, impurities in the deployed scrubbers or effects due to the instrumental components (e.g., O-rings, tubing). However, even if these uncertainties are hard to quantify, they may account for up to a few  $\text{cm}^3$ , against collected sample volumes ranging roughly between 800 – 1600  $\text{cm}^3$ . Therefore, we assume that differences due to instrumental effects remain marginal, while we believe that the day-to-day variability and long-term trends in COS mole fractions are the most important cause for the observed differences.

**Table 3: data gaps caused by clear contamination effects and their respective causes in different AirCore profiles.**

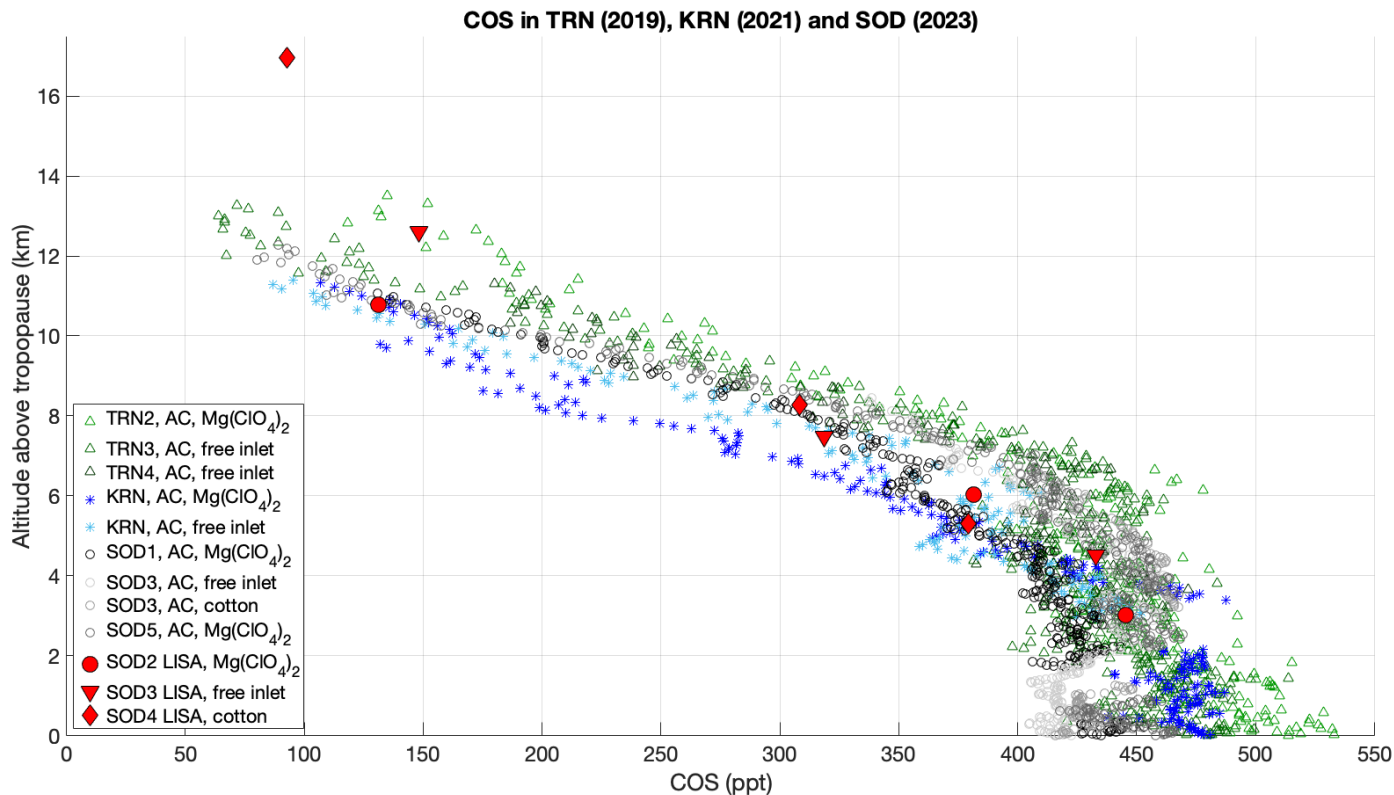
Flight identifier and AirCore inlet	Data gaps	Contamination points along the coil
-------------------------------------	-----------	-------------------------------------

TRN4 – Mg(ClO <sub>4</sub> ) <sub>2</sub>	9.2 – 13.9 km	Glue connection between tubes of different diameter in the coil
KRN – Mg(ClO <sub>4</sub> ) <sub>2</sub>	12.7 – 13.9 km	Glue connection between tubes of different diameter in the coil
SOD1 – Mg(ClO <sub>4</sub> ) <sub>2</sub>	11.9 – 12.8 km	Differential pressure sensors
SOD3 – cotton	4.0 – 5.0 km 7.4 – 8.3 km 11.1 – 12.3 km 16.5 – 17.9 km 20.4 – 21.3 km	Valve employed in O <sub>2</sub> spiking technique to retrieve altitude, or reactions of other species with O <sub>2</sub> itself
SOD5 – Mg(ClO <sub>4</sub> ) <sub>2</sub> and cotton	12.4 – 13.7 km	Differential pressure sensors

The two SOD3 profiles sampled with University of Bern’s double-sided AirCore are of particular interest, since one side was equipped with a cotton-based O<sub>3</sub> scrubber and the other side was left with a free inlet. As reported in Table 3, the spiking technique deployed by the University of Bern caused COS anomalies in one of the profiles. Moreover, as explained in Sect. 2.1.1, the effect of fill gas was amplified for this sampler: the correlation between CH<sub>4</sub> and N<sub>2</sub>O (Fig. S18 in the Supplement) shows a clear deviation for N<sub>2</sub>O mole fractions lower than 280 ppb (corresponding to an altitude of roughly 18 km). This prevented a reasonable analysis of possible effects of O<sub>3</sub> and/or of the efficiency of the cotton scrubber. However, the resulting (shortened) COS profiles show very good accordance with the profiles obtained from other AirCores and small differences ranging between 17 – 46 ppt with the comparable LISA samples (Table 2).

Since it has been shown that O<sub>3</sub> daily variability can affect oxidizable species (Dirksen et al., 2011; Li et al., 2021), we also speculated that part of the differences between the measured profiles may be ascribed to a daily cycle, similarly to what happens for O<sub>3</sub> (Frith et al., 2020; Li et al., 2021; Schranz et al., 2018; Studer et al., 2014). Suggestions of a correlation between COS and O<sub>3</sub> stratospheric chemistry and abundance have been presented in previous studies (Engel and Schmidt, 1994). OH• and O•, known to cause COS loss (Brühl et al., 2012; Chin and Davis, 1995; Krysztofiak et al., 2015), are part of the Chapman cycle of O<sub>3</sub> (Frith et al., 2020; Studer et al., 2014). O<sub>3</sub> daily variability is reported to change depending on seasonality (daily patterns in solar radiation, photolysis), latitude, temperature and atmospheric pressure level (Frith et al., 2020; Studer et al., 2014). However, reaction kinetics and the current estimates of stratospheric COS sinks of  $50 \pm 15$  GgS yr<sup>-1</sup> due to photolysis (Whelan et al., 2018) do not support the hypothesis of a detectable daily cycle with the methods presented in this study. On top of that, since we are uncertain about the effectiveness of the cotton-based scrubbers deployed during our campaigns and as we have no O<sub>3</sub> measurements, we cannot support this hypothesis.

370 Overall, we consider our results to be a trustworthy representation of the COS stratospheric conditions during sampling. In fact, in spite of the observed differences between the retrieved profiles, all profiles show similar trends when compared with one another and with the LISA samples, too. All measurements show the expected stratospheric sink clearly. Their agreement with SPIRALE and ACE-FTS observations will be discussed in Sect. 4.2 and 4.3, respectively.



375 **Figure 2: COS profiles and samples from all campaigns, plotted against altitude above tropopause.**

#### 4.2 Comparison with SPIRALE observations

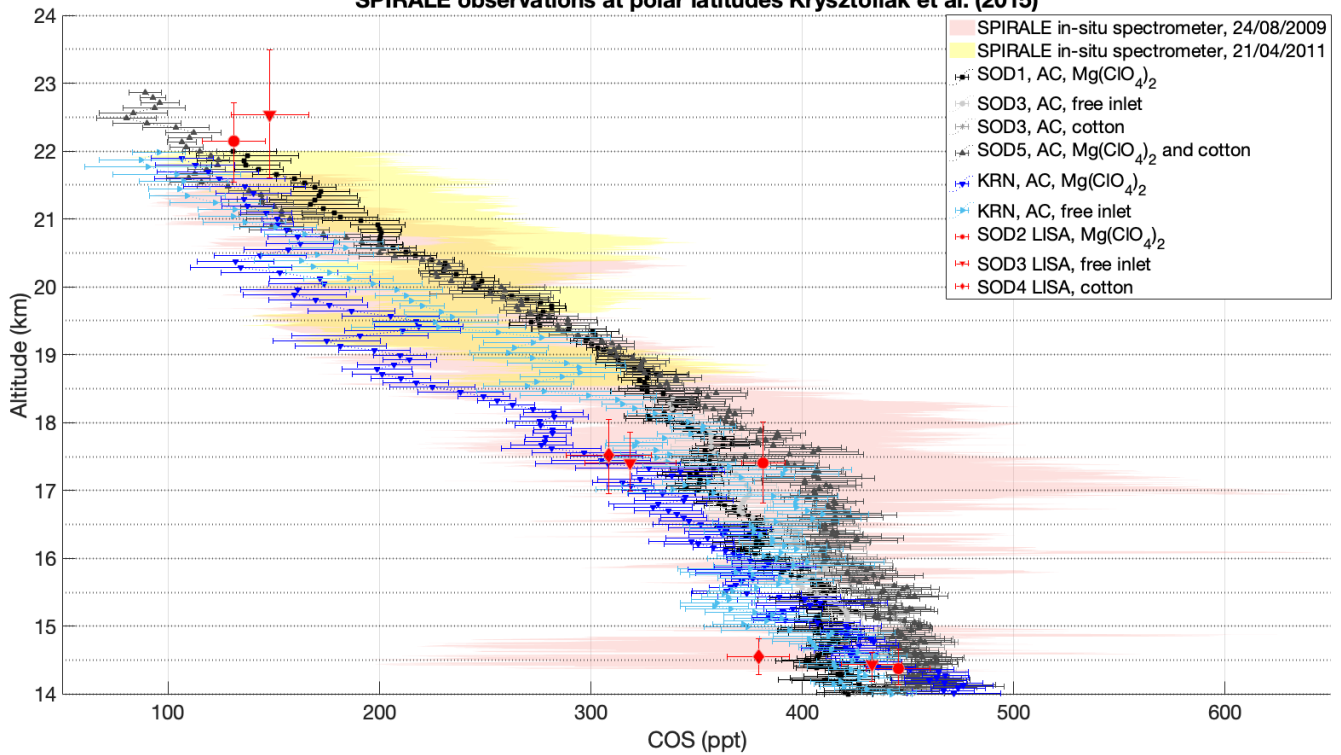
Figure 3 and Figure 4 show a comparison plot of AirCore and LISA observations with the in situ SPIRALE COS observations realised by Krysztofiak et al. (2015) in 2009 and 2011. It is evident that SPIRALE observations are only available between 14.5 and 22 km. These observations have a higher spatial resolution over the vertical column (3 to 5 m), but are associated to lower precision compared to AirCore COS measurements analysed by QCLS. Moreover, both techniques measure profiles that are specific for the location and the time where the measurement occurs. In this case, both studies have data collected at polar latitudes, although at different times of the year and, most importantly, between 10 and 14 years apart from each other. However, it is relevant to mention that no significant trends were observed for stratospheric COS in recent years (Barkley et al., 2008; Coffey and Hannigan, 2010; Rinsland et al., 2008; Toon et al., 2018). To realise a meaningful comparison, both AirCore profiles and SPIRALE observations have been averaged over 0.5 km bins. Using the averaged bins, a linear regression was performed and the difference between AirCore and SPIRALE was calculated. As shown in Figure 3 and Figure 4, most

AirCore profiles and all the LISA samples collected at altitudes comparable to the SPIRALE datasets fall within the uncertainty range of both SPIRALE profiles. The horizontal error bars reported in Figure 3 represent the uncertainty of QCLS measurements, while the ones in Figure 4 are the standard deviation obtained from the averaging of SPIRALE over LISA's  
390 sampling altitude intervals and AirCore profiles over 0.5 km altitude intervals. The shaded areas in Figure 4 correspond to SPIRALE's errors.

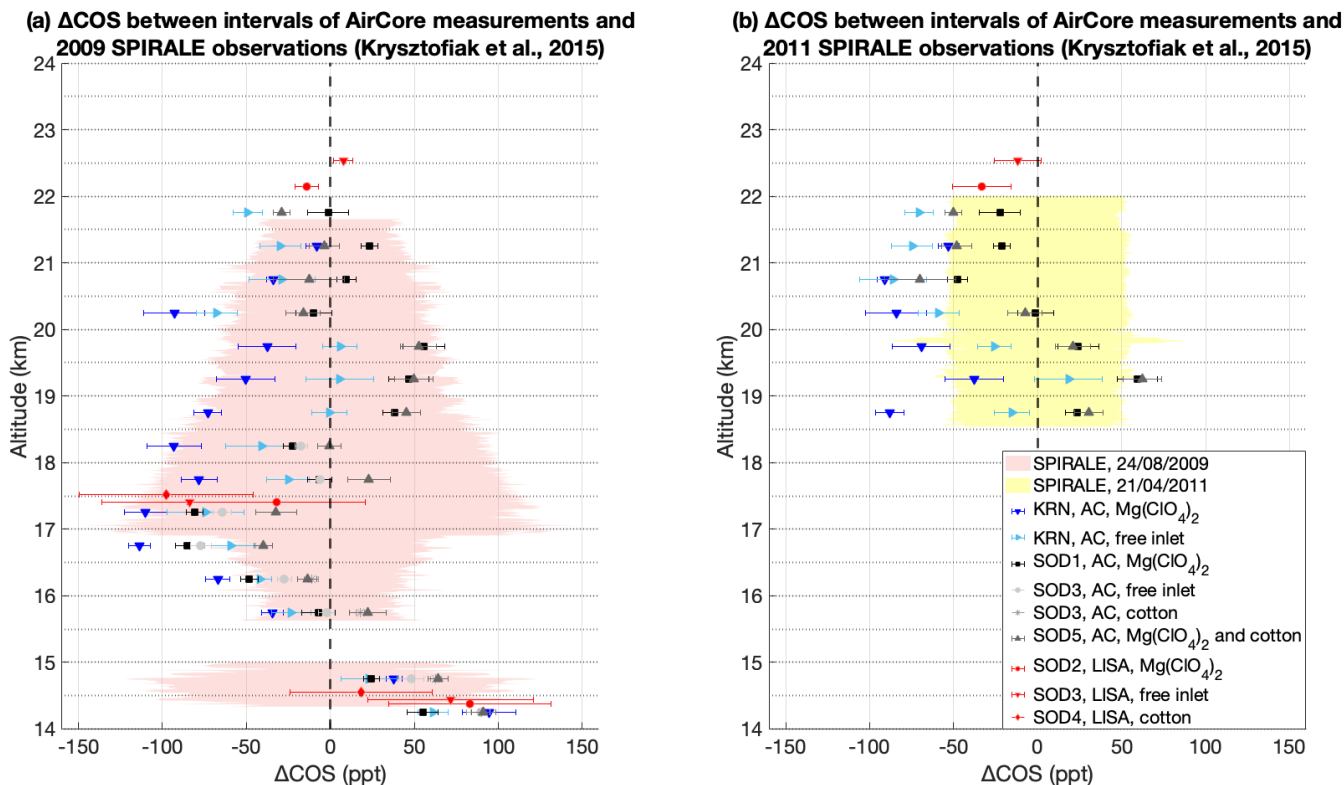
Figure 5 and Table 5 show plots and results of the linear regressions of AirCore and LISA vs. SPIRALE observations in 2009 and 2011, respectively. The linear regression of averaged KRN and SOD observations against SPIRALE's 2009 observations  
395 leads to  $R^2$  values above 0.7 for both AirCores and LISA, with a slope of  $0.921 \pm 0.061$  and  $0.892 \pm 0.230$  respectively. This, in spite of the time span between the two experiments, indicates a high correlation between the methods, with AirCore results being approximately 8% lower than SPIRALE's 2009 observations, while LISA's regression slope suggests a 11% bias but does not significantly differ from 1. Between 15.5 and 17.5 km, differences between 40 – 110 ppt can be seen between  
400 both KRN and SOD AirCore profiles and the 2009 SPIRALE. However, in this range (in particular between 15.8 and 16.2 km), SPIRALE measured a COS spike that reached up to 577 ppt, a rather unusual mole fraction for these altitudes, which is reflected also in a previous comparison between SPIRALE and ACE-FTS (see Fig. 5 in Krysztofiak et al., 2015). Moreover, as reported in Fig. 5 of Krysztofiak et al. (2015), SPIRALE results fall generally above the averaged ACE-FTS observations. Unfortunately, only COS measurements are available from SPIRALE and it is not possible to verify this idea with observations of other tracers. Nevertheless, considering day-to-day variability (e.g. discrepancies in tropopause height, or the above-cited  
405 air transport), the 12 to 14 years differences between the campaigns and the long-term trends occurred in this time span (Bernath et al., 2020; Glatthor et al., 2017; Hannigan et al., 2022; Kremser et al., 2015; Lejeune et al., 2017), the linear regressions suggest a strong agreement between the datasets, with the AirCore and LISA results being generally lower than SPIRALE results in 2009.

410 With regard to SPIRALE observations in 2011, the linear regression could be only performed on 27 averaged AirCore COS mole fractions from the KRN and SOD campaigns and resulted in a weaker correlation between this dataset and our results compared to the 2009 observations. This could be due to the limited altitudinal range of these observations and due to the different sampling season (April for this SPIRALE measurements, August for our campaigns), on top of the reasons mentioned earlier in the text for the differences between our data and the SPIRALE 2009 observations. Nevertheless, at polar latitudes  
415 we observe COS mole fraction decreasing from an all-campaign average of  $421 \pm 26$  ppt below 17 km to  $170 \pm 41$  ppt between 20 – 22 km (see Figure 3). This is comparable to the decrease from 460 to 150 ppt reported by Krysztofiak et al. (2015) and from 440 to 120 ppt reported by and Leung et al. (2002).

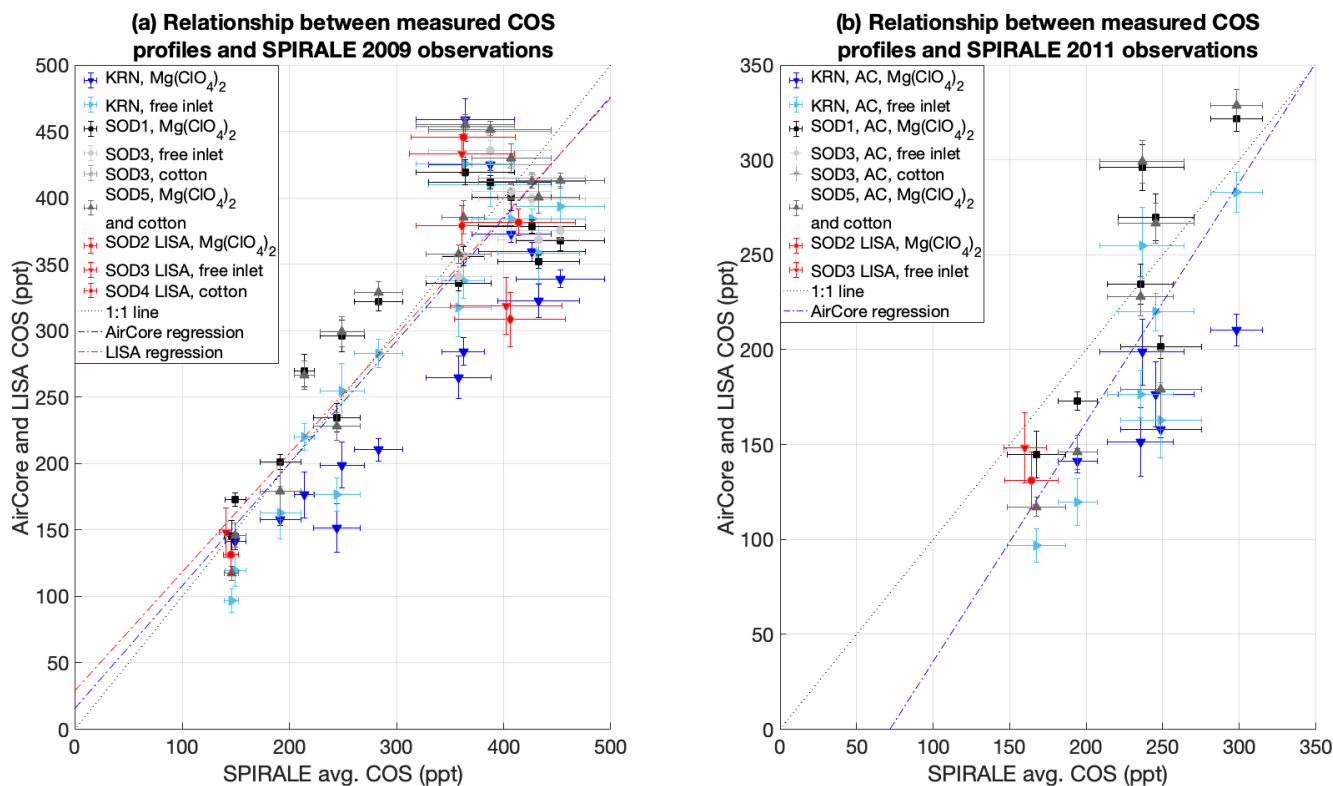
**AirCore profiles and LISA samples vs.  
SPIRALE observations at polar latitudes Krysztofiak et al. (2015)**



420 **Figure 3: measured COS profiles and LISA samples at polar latitudes (Kiruna - KRN, Sodankylä - SOD), compared with the SPIRALE's in situ observations from flights in KRN (red and yellow shading representing COS  $\pm$  std. dev.), presented by Krysztofiak et al. (2015). The dotted horizontal lines signal the intervals within which the average COS mole fraction is calculated (see Figure 4). The horizontal error bars represent the uncertainty of QCLS measurements.**



425 **Figure 4:** measured COS profiles and LISA samples at polar latitudes (Kiruna - KRN, Sodankylä - SOD), compared with the SPIRALE's in situ observations from flights in KRN (red and yellow shading representing COS  $\pm$  std. dev.), presented by Krysztofiak et al. (2015). The dotted horizontal lines signal the intervals within which the average COS mole fraction is calculated. Panels (a) and (b) show the difference between the measured AirCore profiles and the SPIRALE results. The error bars correspond to the standard deviation obtained from the averaging of SPIRALE over LISA's sampling altitude intervals, and over AirCore profiles over 0.5 km altitude intervals.



430

Figure 5: linear regressions between SPIRALE observations (panel a, 2009 and panel b, 2011) and AirCore and LISA samples. The dotted black line represents the 1:1 line. In panel (b) the regression between LISA samples and SPIRALE averaged COS mole fractions was not possible, since only two data points collected at similar altitudes were comparable. The statistical values related to these regressions are reported in Table 4.

435

Table 4: summary of the performed linear regressions between measured samples and SPIRALE in situ spectrometry COS observations (see Figure 5).

Independent variable	Dependent variable	Slope	Intercept	Number of observations	R <sup>2</sup>
SPIRALE 2009	KRN and SOD AirCore observations	$0.921 \pm 0.061$	$16 \pm 21$	71	0.766
SPIRALE 2009	SOD LISA observations	$0.892 \pm 0.230$	$29 \pm 79$	8	0.714
SPIRALE 2011	KRN and SOD AirCore observations	$1.26 \pm 0.23$	$-90 \pm 56$	27	0.533

SPIRALE 2011	SOD LISA observations	-	-	2	-
--------------	-----------------------	---	---	---	---

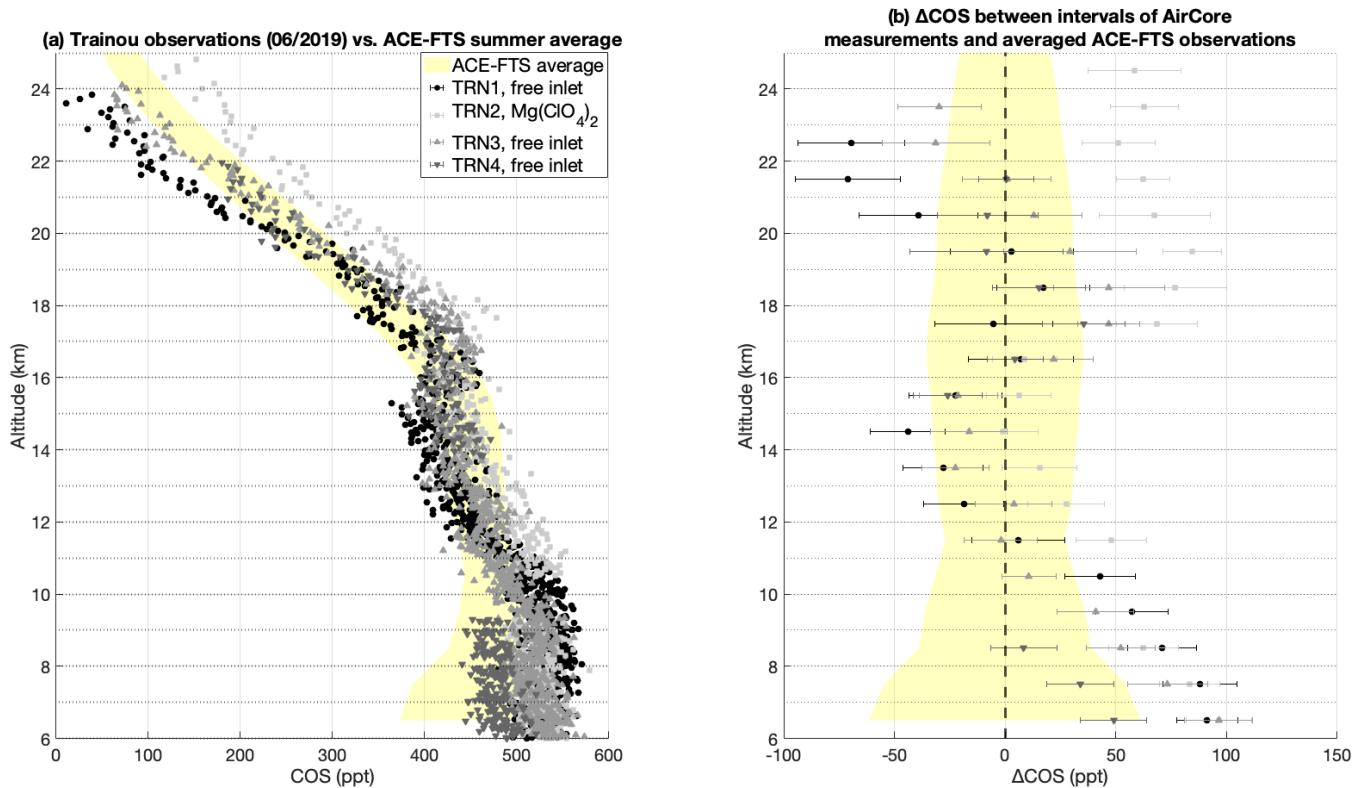
### 4.3 Comparison with ACE-FTS observations

Figure 6 and Figure 7 show the comparison of the measured TRN, KRN and SOD AirCore profiles with the ACE-FTS v5.3 (Boone et al., 2023; Schmidt et al., 2024) averaged observations, while Figure 8 and Table 5 show the results of the linear regression models of both campaigns. The agreement between the averaged ACE-FTS profiles and the AirCore profiles is rather coherent at both mid and polar latitudes. The TRN data shows good agreement between ACE-FTS and AirCore profiles, in particular in the stratospheric part of the profile, where most differences fall within the  $\pm 50$  ppt range. The biggest discrepancies are found in the tropospheric part, where seasonal variabilities and daily variations are more pronounced. At polar latitudes, the profiles measured in KRN in 2021 show better agreement with the ACE-FTS results, while the SOD measurements generally resulted in higher COS mole fractions above 15 km altitude, with differences up to  $\sim 80$  ppt. This may be due to specific conditions during the period when the flights were performed, such as different atmospheric transport patterns, or the uncertainties in the AirCore methodology described in Sect. 4.1.3. Similarly to what has been described in Sect. 4.2, linear regressions between ACE-FTS and AirCore and LISA samples were performed to quantify the level of agreement between the results. In this case, AirCore profiles were averaged over 1 km intervals to make them comparable to the ACE-FTS resolution.

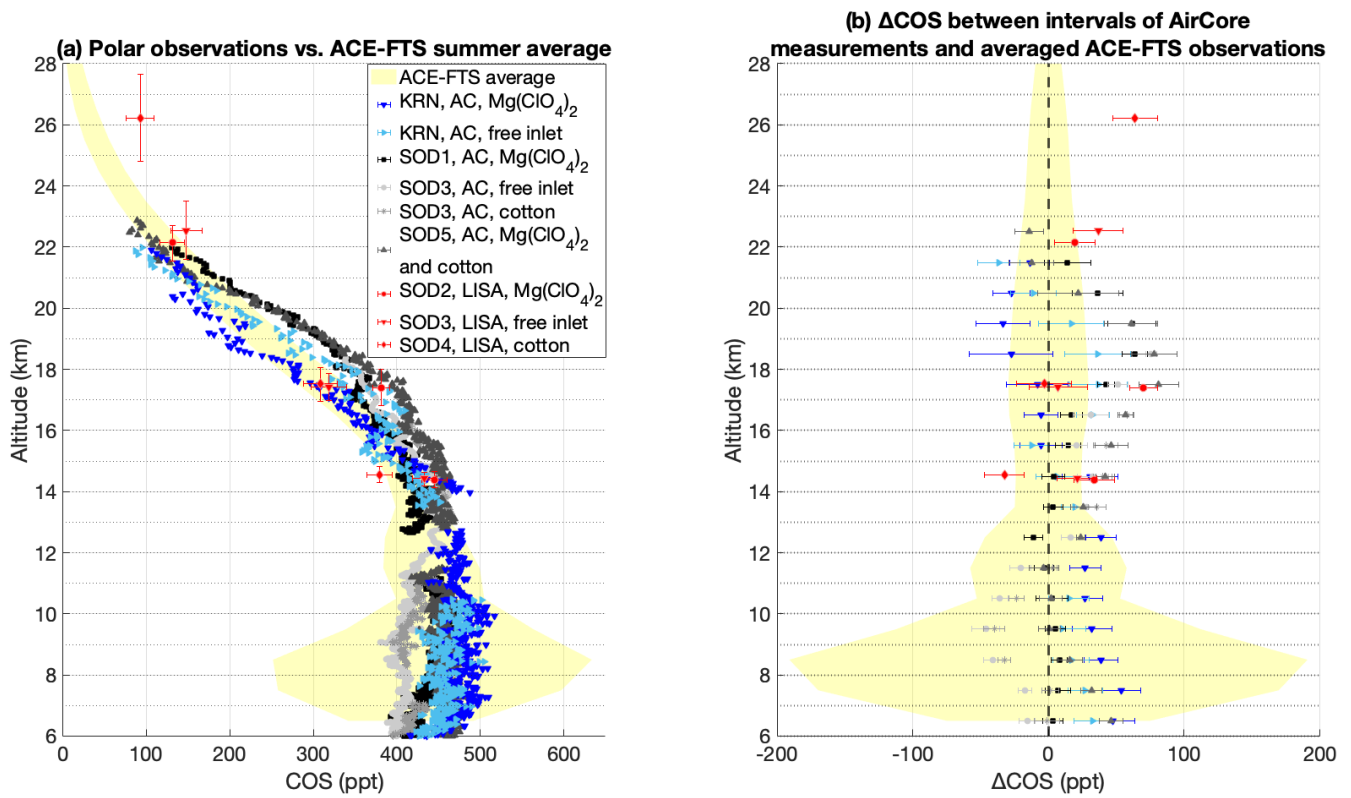
The linear regressions (Figure 8) between polar summer ACE-FTS average and AirCore profiles from all the campaigns at polar latitudes resulted in high correlations ( $R^2$  values  $> 0.9$ ) and a slope signalling a difference of roughly 5% between the two methods. Consistently, the linear model applied to the mid-latitude ACE-FTS selection and the TRN AirCore profiles resulted in high correlation and a difference of roughly 5%. The regression between SOD LISA results and the ACE-FTS instead suggests a difference of roughly 10% with a slightly lower correlation which may be due a higher COS measured in the highest measured sample not flagged as outlier, SOD4 – L4, compared to the ACE-FTS average (93 ppt against 29 ppt). The removal of this sample from the regression leads to a difference of less than 7%. The resulting intercept of the regression between polar ACE-FTS data and polar LISA samples is significantly higher than 0, suggesting slightly higher estimates of COS mole fraction with LISA compared to ACE-FTS when approaching low COS levels. However, the estimated slopes indicate that the data difference with ACE-FTS over altitude is less than 5% for AirCores and roughly 10% for LISA.

Most profiles show higher COS mole fractions in the 14 – 24 km range at polar latitudes and in the 16 – 24 km range at mid-latitudes when compared to ACE-FTS averages. Glatthor et al. (2017) reported a difference up to 100 ppt between COS mole fraction retrieved from MIPAS remote sensing and the ACE-FTS ones between 13 – 16 km. Velazco et al. (2011) found COS mole fractions 15% higher than in situ spectrometry and ACE-FTS profiles, while Krysztofiak et al. (2015) reported

consistency within 11% at polar latitudes and a positive difference of 15 – 20% at mid-latitudes, taking into account both instrumental uncertainties. The discrepancy we observe between AirCore profiles and ACE-FTS is in the range of 80 ppt and maximises between 17 – 22 km. Nonetheless, some profiles show lower COS mole fractions in the same ranges. Therefore, the differences are either due to day-to-day variability, or due to instrumental issues, such as different scrubbers that were employed in different flights.



475 **Figure 6: comparison of the AirCore profiles in Trainou (TRN) with ACE-FTS average over summer months between 45 – 49° N in the 2012 – 2024 period. In panel (a), the shaded yellow area represents the averaged ACE-FTS results  $\pm 1\sigma$ . The dotted horizontal lines signal the intervals within which the average is calculated. In panel (b), the shaded area corresponds to ACE-FTS 0 difference,  $\pm 1\sigma$ . The error bars in panel (b) correspond to the standard deviation obtained averaging AirCore profiles over 0.5 km altitude intervals.**



480

Figure 7: comparison of the AirCore profiles (Kiruna - KRN, Sodankylä - SOD) and LISA samples with ACE-FTS average over summer months at 65 – 69° N in the 2012 – 2024 period. In panel (a), the shaded yellow area represents the averaged ACE-FTS results  $\pm 1\sigma$ . The dotted horizontal lines signal the intervals within which the AirCores' average is calculated. In panel (b), the shaded area corresponds to ACE-FTS 0 difference,  $\pm 1\sigma$ . The error bars in panel (b) correspond to the standard deviation obtained averaging AirCore profiles over 0.5 km altitude intervals.

485

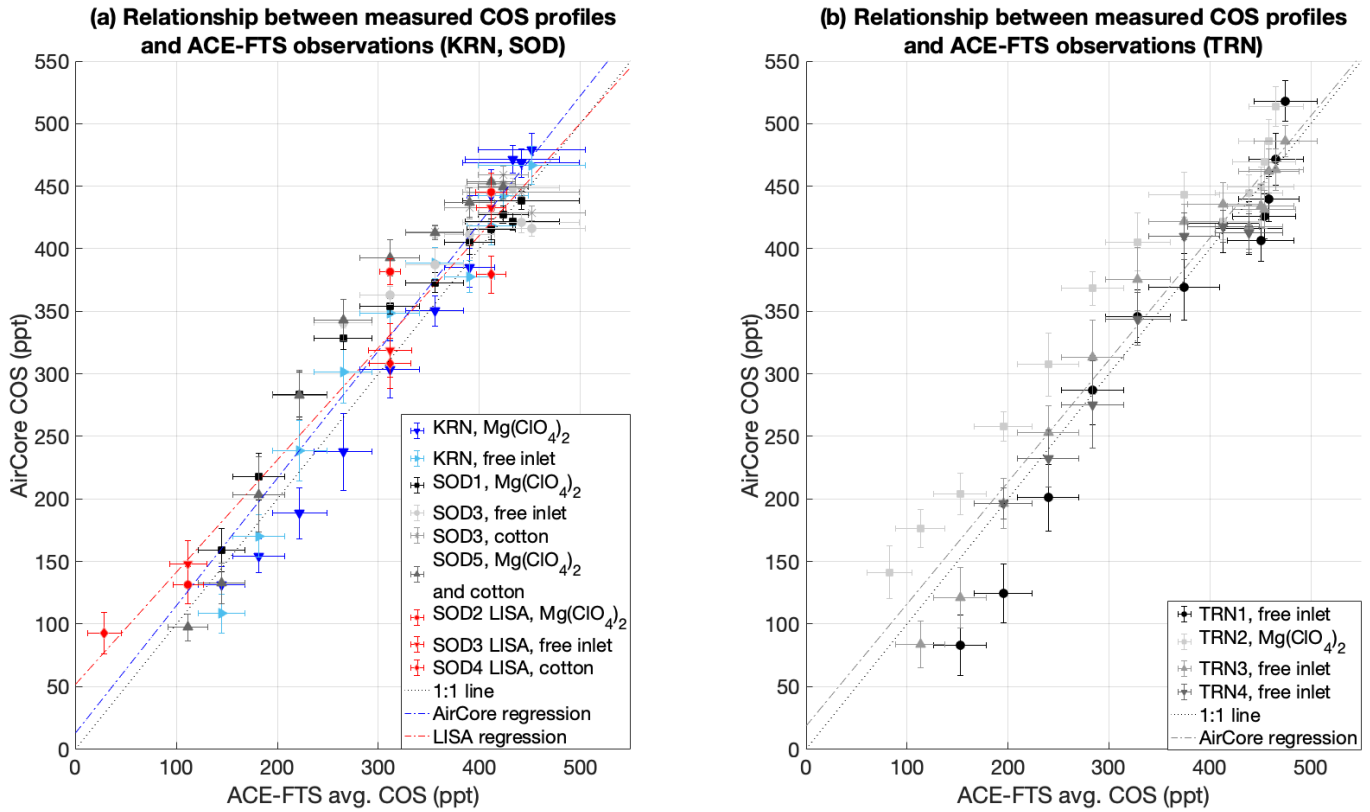


Figure 8: linear regressions between ACE-FTS averaged observations and AirCore and LISA samples at polar latitudes (KRN and SOD, panel a) and at mid latitudes (TRN, panel b). The dotted black line represents the 1:1 line. The statistical values related to these regressions are reported in Table 5.

490 Table 5: summary of the performed linear regressions between measured samples and previous ACE-FTS COS remote sensing observations (see Figure 8).

Independent variable	Dependent variable	Slope	Intercept	Number of observations	R <sup>2</sup>
ACE-FTS “TRN” average	TRN AirCore observations	$0.975 \pm 0.045$	$18 \pm 16$	48	0.911
ACE-FTS “polar” average	KRN and SOD AirCore observations	$1.019 \pm 0.040$	$13 \pm 14$	57	0.923
ACE-FTS “polar” average	SOD LISA observations	$0.897 \pm 0.072$	$52 \pm 22$	9	0.957

## 5. Conclusion

This study presented in situ stratospheric COS observations based on collected air samples using two new techniques, AirCore and (Big)LISA samplers. The collected continuous and discrete stratospheric samples were analysed with a QCLS in the CIO  
495 laboratory at the University of Groningen. The results obtained with both techniques closely resemble the stratospheric trends retrieved from previous discrete samples and in situ spectroscopic observations. Moreover, we found less than 5% difference between AirCore data and averaged ACE-FTS data obtained with remote sensing, although we observe higher COS estimations when approaching low COS abundances when compared to ACE-FTS. We found that, when deploying MLF bags to measure  
500 COS, it is necessary to pre-treat the bags before flight to prevent COS contamination due to outgassing from the polymers constituting the bag. We also found that cotton-based O<sub>3</sub> scrubbers may have limited efficiency, especially when cotton has been in contact with the air for several months. Squalene-based scrubbers showed excellent O<sub>3</sub> scrubbing performances and seemed to have no effect on COS abundance and may become a valuable addition to stratospheric samplers that require O<sub>3</sub> removal.

505 We found no clear evidence that stratospheric O<sub>3</sub> causes positive or negative biases in COS measurements, since no repeatable differences were found in our samples while deploying different sorts of inlets with different O<sub>3</sub> scrubber materials. However, the observed COS mole fractions showed some day-to-day variability, a hypothesis which may be ascribed to stratospheric transport or instrumental biases. Consistent differences in COS profiles point to observed transport variability, hypothesis that may be corroborated by modelling efforts. The investigation on the effects of O<sub>3</sub> on air samples, in particular containing  
510 reduced sulfur species, could be facilitated by the deployment of the squalene-based scrubbers.

## Appendix A

### Ozone scrubbing materials

O<sub>3</sub> is a reactive gas species that can be found at mole fractions up to about 8 ppm in the stratosphere, where it is formed by the  
515 interaction of atmospheric O<sub>2</sub> with UV radiation (Bernhard et al., 2023). O<sub>3</sub> is a strong oxidant and can react with other trace gases, including reduced sulfur compounds such as dimethyl sulfide (DMS) and carbon disulfide (CS<sub>2</sub>) (Andreae et al., 1985; Hofmann et al., 1992; Persson and Leck, 1994). Moreover, the oxidation of DMS and CS<sub>2</sub>, indirect precursors of COS, was reported as a potential bias of tropospheric COS measurements obtained after cryogenic sampling (Hofmann et al., 1992). On top of this, the amount of COS was found to be lower if sampled in presence of O<sub>3</sub> (Engel and Schmidt, 1994). Therefore, a  
520 number of oxidant removal substances, such as manganese dioxide (MnO<sub>2</sub>), cotton wadding, sodium carbonate (Na<sub>2</sub>CO<sub>3</sub>), potassium hydroxide (KOH) or a KI/glycerol/Vitex solution have been deployed to remove oxidants during cryogenic sampling, in both tropospheric and stratospheric applications (Andreae et al., 1985; Engel and Schmidt, 1994; Hofmann et al.,

1992; Persson and Leck, 1994 and references therein). Among these, scrubbers based on cotton wadding were tested and proved to be effective for tropospheric cryogenic samples (Hofmann et al., 1992; Persson and Leck, 1994). However, only MnO<sub>2</sub> has been deployed for stratospheric applications (Engel and Schmidt, 1994). Therefore, we tested multiple substances for their O<sub>3</sub> scrubbing efficiency and their influence on the mole fractions of the analysed gases. During the first laboratory tests, we found that MnO<sub>2</sub> interacted strongly with multiple tracers. In order to find a suitable O<sub>3</sub> scrubber that would perform well under stratospheric conditions, we conducted a series of experiments, as described below.

We designed an experimental setup (Figure A1) that obtains an air mixture with high O<sub>3</sub> at low pressure and low temperature, to assess the performance of O<sub>3</sub> scrubbers under stratospheric air conditions. Air from a laboratory-made synthetic air (~79% N<sub>2</sub>, ~21% O<sub>2</sub>) cylinder containing mole fractions of the measurable tracers, close to stratospheric conditions (1435.7 ppb CH<sub>4</sub>, 0 ppb N<sub>2</sub>O, 392.67 ppm CO<sub>2</sub>, 0 ppt COS, and 0 ppb CO), was flowed through a custom-made Y-shaped quartz tube, which passed through a UV lamp that served as an O<sub>3</sub> generator. With a QCLS-controlled mass flow of 50 mL min<sup>-1</sup> and a path length of about 6 inches (~ 15.2 cm) through UV radiation, it was possible to generate up to 3500 – 4000 ppb O<sub>3</sub>. The air could be directed to each side alternately using a three-way valve, allowing measurements of the air after O<sub>3</sub> generation, with or without an oxidant scrubber. The tube passed through a polystyrene box, where 193 K freeze packs could be inserted to simulate low- to mid-stratospheric temperatures (air temperature could reach as low as roughly 213 K). The flow and pressure of the air in the sampling lines were controlled by the QCLS frontend, with the mass flow typically maintained at 50 mL min<sup>-1</sup> and the pressure reaching as low as 250 hPa. A bypass channel directly connected to the QCLS was also available for reference measurements.

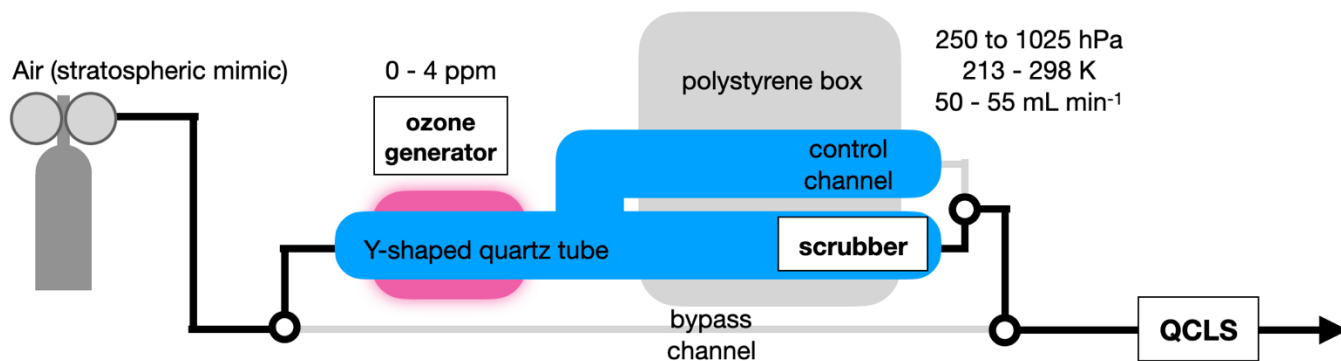


Figure A1: the experimental setup for the O<sub>3</sub> scrubber testing. The black circles represent three-way valves. Apart from the quartz tube, all connections were realised with stainless steel tubing.

The initial tests focused only on the performance of O<sub>3</sub> scrubbers based on cotton, supported by available research on the consumption of O<sub>3</sub> by contact with fabrics (Andreae et al., 1993; Coleman et al., 2008; Hofmann et al., 1992; Persson and Leck, 1994). Surgical cotton wool (approximately 3 - 10 g of cotton) was inserted on one side of the Y-shaped quartz tube.

While cotton scrubbers seemed to work initially (Table A1), in later tests it was noticed that cotton would quickly lose efficiency, in particular after some storage time. While “new” cotton pads still exhibited some O<sub>3</sub> scrubbing capacity, the same pads, after storage (“old” cotton), showed almost no scrubbing ability.

It was observed that the efficiency of O<sub>3</sub> scrubbing changed significantly depending on whether nitrile gloves were used or not while handling the cotton pads. This led to the hypothesis that O<sub>3</sub> was mostly removed by reaction with skin oils rather than with the cotton itself. This hypothesis was further supported by existing literature (Coffaro and Weisel, 2022; Coleman et al., 2008; Zhou et al., 2016). Following Coffaro and Weisel (2022), knowing that squalene, a triterpene, accounts for 12% of skin oils composition (Picardo et al., 2009), squalene-based scrubbers were also tested. Consequently, the potential impacts of the reaction between O<sub>3</sub> and squalene on other trace gases were investigated. The squalene-based O<sub>3</sub> scrubbers consisted of one drop of laboratory-quality squalene (Sigma-Aldrich, ≥ 98%) deposited with a Pasteur pipette on glass wool, which had been previously proven inert to the analysed trace gases.

We designed the final experimental setup with five possible configurations:

- a. No O<sub>3</sub> generation, air flowed through the control channel
- b. O<sub>3</sub> generation, air flowed through the control channel
- c. No O<sub>3</sub> generation, air flowed through the cotton/squalene scrubber
- d. O<sub>3</sub> generation, air flowed through the cotton/squalene scrubber
- e. Total bypass channel

The data from the experimental time series was selected and designated to the respective configuration. These configurations were then used as categorizations to perform an ANOVA test, which would eventually corroborate significant differences between each species’ mole fraction, depending on the experimental configuration. The results are presented and discussed in the following paragraphs. The ANOVA test results on the effect of the squalene scrubbers on other tracers are reported in Sect. S3 in the Supplement.

The possible coincidental removal of COS by squalene and cotton was assessed just briefly with the same experimental setup described above, placing squalene in one channel and cotton in the other. For this test, a tropospheric compressed air mixture (2201.3 ppb CH<sub>4</sub>, 338.9 ppb N<sub>2</sub>O, 430.10 ppm CO<sub>2</sub>, 747 ppt COS, and 180.6 ppb CO) was employed. The findings for COS and O<sub>3</sub> are presented at the end of the Results section of this Appendix.

### **Results of tests on O<sub>3</sub> scrubbers**

As reported in Table A1, the initial tests on cotton O<sub>3</sub> scrubbers (performed in 2023) resulted in the quantitative removal of about 3.5 ppm O<sub>3</sub>, lasting up to roughly 2.5 to 40 L of air with a flow rate of 50 mL min<sup>-1</sup>, depending on the amount of cotton used. However, months later, cotton pads from the same bag lost their scrubbing capacity after only about 0.05 to 0.75 L of

585 air, soon showing a clear drop in performance and allowing progressively more O<sub>3</sub> to pass through. As explained in Sect. 2.3, it was observed that the efficiency of O<sub>3</sub> removal was significantly higher when the cotton was handled with bare hands and eventually led to squalene-based scrubbers.

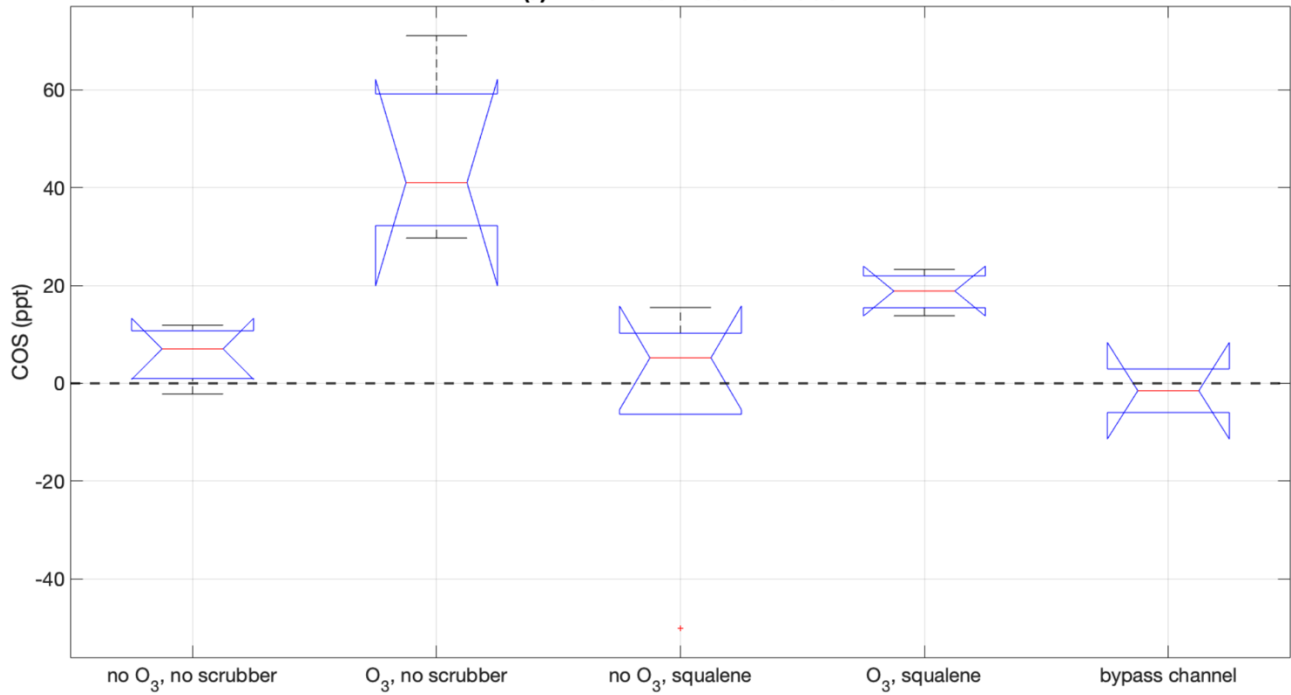
590 We found that one drop of squalene from a Pasteur pipette on glass wool was sufficient to quantitatively remove O<sub>3</sub> up to roughly 12 L of air without showing any sign of O<sub>3</sub> breakthrough (and we speculate it could have possibly scrubbed for an even longer duration). When no O<sub>3</sub> was generated, no significant differences were observed for COS, indicating that nor cotton, nor squalene caused COS contaminations when interacting with the air samples.

**Table A1: summary of the first experiments regarding O<sub>3</sub> scrubbers, which eventually led to the choice of focusing on squalene-based scrubbers for the laboratory tests.**

<b>Scrubber type</b>	<b>Capacity of scrubbing ~3.5 ppm O<sub>3</sub> (air volume)</b>	<b>Influence on O<sub>3</sub></b>	<b>Influence on COS</b>
“Old” cotton, handled with gloves (1 cotton pad, ~ 0.3 g of cotton)	~ 50 – 750 mL	Quantitative removal at the beginning, followed by progressive O <sub>3</sub> increase	Not significant, as long as the scrubber worked
“Old” cotton, handled with bare hands (1 cotton pad, ~ 0.3 g of cotton)	≥ 5000 mL	Quantitative removal	Not significant
“New” cotton, handled with gloves (1 cotton pad, ~ 0.3 g of cotton)	~ 800 - 2500 mL	Quantitative removal at the beginning, followed by progressive O <sub>3</sub> increase	Not significant, as long as the scrubber worked
Squalene (1 Pasteur-pipette drop, ~ 0.05 mL, on rock wool)	≥ 12000 mL	Quantitative removal	Not significant
No scrubber	-	~3.5 ppm measured	0 – 40 ppt increase

595

(a) ANOVA test results for COS



(b) ANOVA test results for O<sub>3</sub>

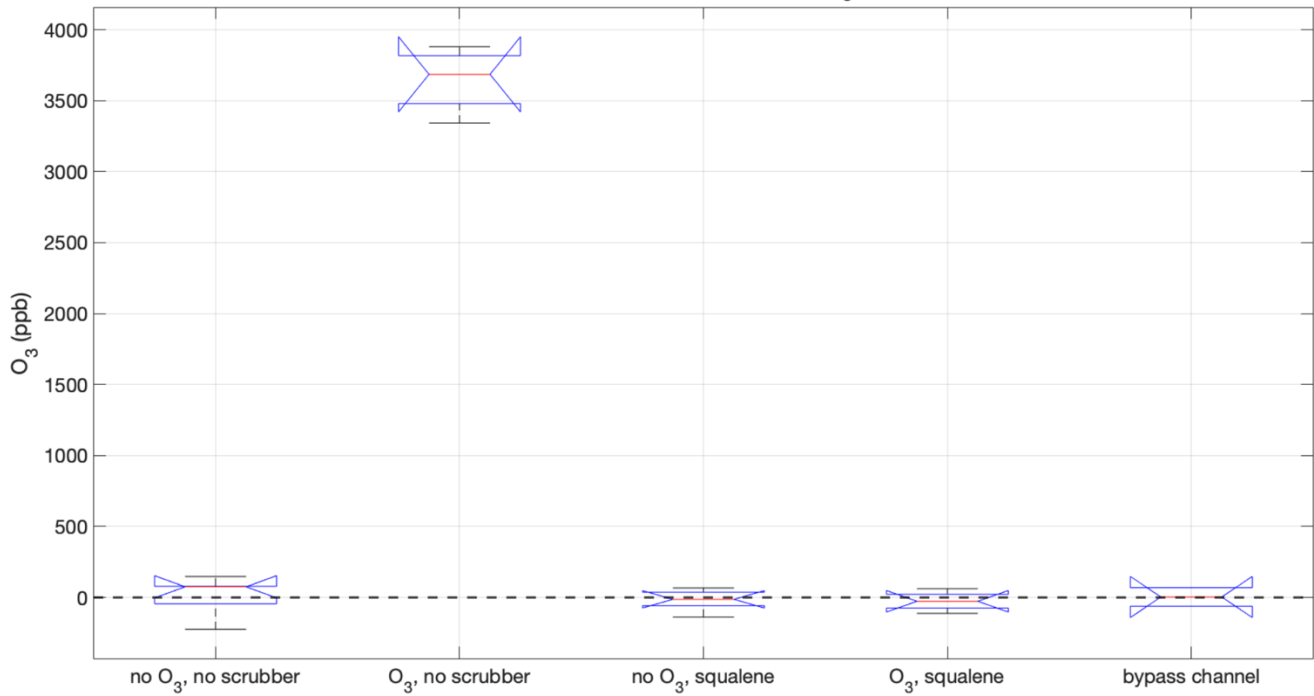


**Figure A2: ANOVA test representation for COS (panel a, top) and O<sub>3</sub> (panel b, bottom). The red lines represent the median, while the edges of the blue boxes correspond to the 25th (bottom) and 75th (top) percentile. Black whiskers extend to most extreme data point.**

600

The results of the ANOVA test on squalene-based scrubbers are represented in Figure A2 for both COS and O<sub>3</sub>. The corresponding p-values are reported in Table S6 and S7 in the Supplement. It is clear that squalene removes O<sub>3</sub> quantitatively: when in place, O<sub>3</sub> mole fraction shows no significant difference between the scrubbing squalene and the configurations where O<sub>3</sub> is not generated (p-value > 0.05).

605

Regarding COS, significant differences (p-value < 0.05) were found between the configuration where O<sub>3</sub> flows through without any scrubber and all other configuration. However, it is noteworthy that significant differences in COS mole fraction were also observed between the configuration where O<sub>3</sub> is generated and then removed by squalene, and the bypass configuration. The air mixture used for this experiment was prepared in the laboratory and contained 0 ppt COS. The possible reasons behind these results are discussed in the following paragraph.

610

The effect of squalene on CO<sub>2</sub>, CO, N<sub>2</sub>O and CH<sub>4</sub> was tested just briefly and is shown in Fig. S1-S4 and Tables S2-S5 in Sect. S2 of the Supplement. Overall, CO trends resembled very closely the ones observed for COS, while no significant variance was observed for all other tracers.

615

The effects of different O<sub>3</sub> scrubbers on COS and O<sub>3</sub>, tested on tropospheric compressed air, are shown in Figure A3 and Figure A4. The p-values of the ANOVA test for each species are reported in Table S8 and Table S9 in the Supplement.

When O<sub>3</sub> was not generated, none of the two scrubbers showed significant differences with the bypass channel neither for COS, nor for O<sub>3</sub>. Clearly, the O<sub>3</sub> scrubbing was performed quantitatively by the squalene-based scrubber, while the cotton-based one was likely saturated and could not remove the vast majority of the produced ozone. When O<sub>3</sub> was produced in the UV lamp, similarly to what happened during the tests on air simulating stratospheric conditions, we measured higher COS molar fractions both with cotton and with squalene.

620

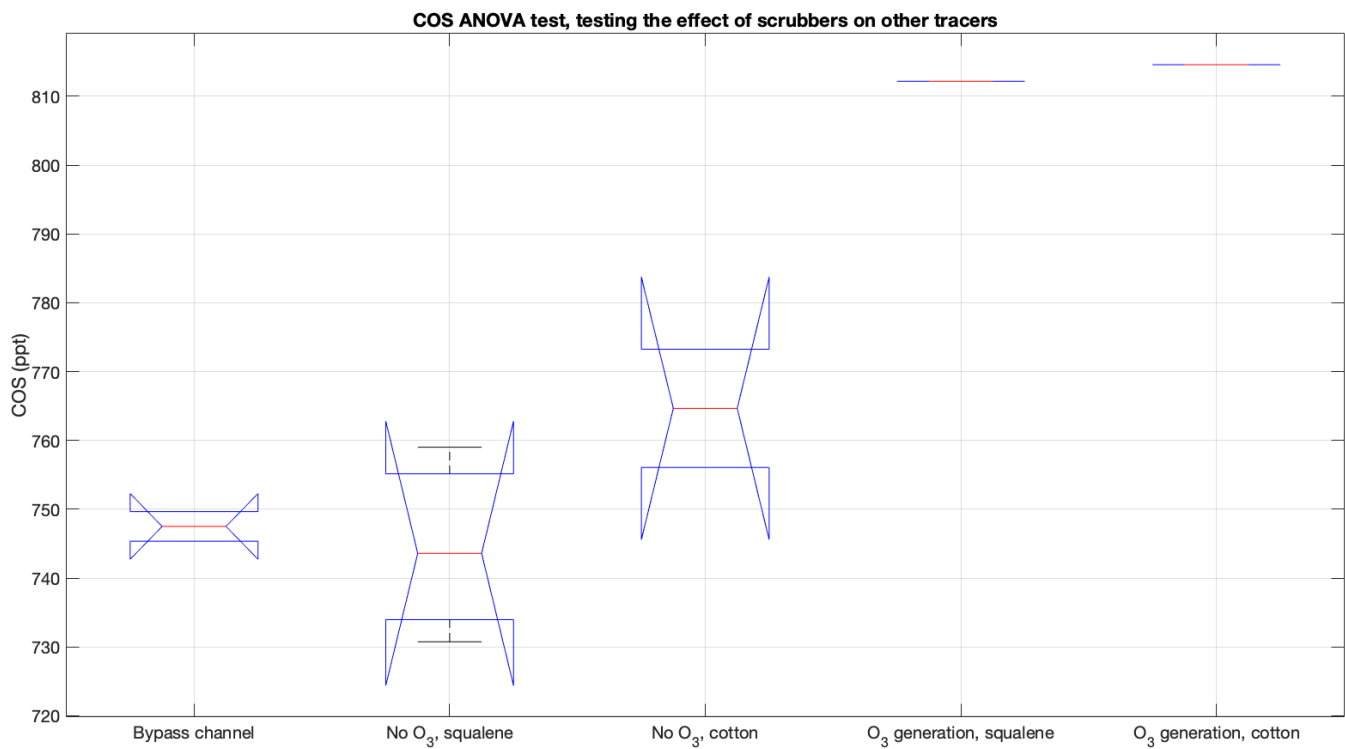
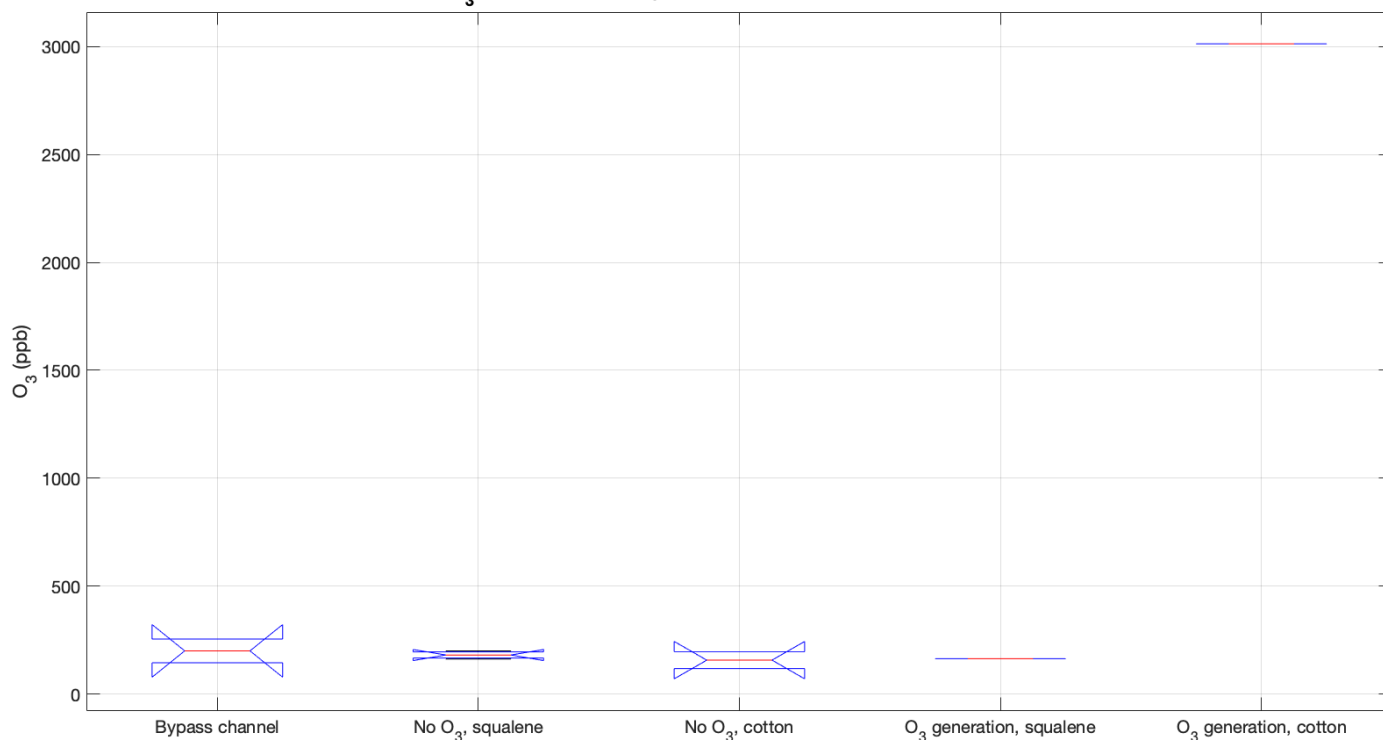


**Figure A3: effects of squalene and cotton O<sub>3</sub> scrubbers on a compressed tropospheric air mixture containing COS.**

**O<sub>3</sub> ANOVA test, testing the effect of scrubbers on other tracers**



625

**Figure A4: effects of squalene and cotton O<sub>3</sub> scrubbers on O<sub>3</sub> in a compressed tropospheric air mixture.**

### **Discussion over the results of tests on O<sub>3</sub> scrubbers**

Our study showed that cotton had only limited O<sub>3</sub> destruction efficiency over time (Table A1), in spite of its employment as an O<sub>3</sub> scrubber for reduced sulfur compounds in previous studies (Andreae et al., 1985; Hofmann et al., 1992; Persson and Leck, 1994). Existing literature reports reactions of cellulose (the primary constituent of cotton) with O<sub>3</sub> leading to the formation of carbonyl and carboxyl groups on cellulose itself (Valls et al., 2022; Zhang et al., 2024). We speculate that the high abundance of O<sub>3</sub> (up to about 3500 ppb) may have saturated the cotton rapidly. This concentration is comparable to that of the stratospheric O<sub>3</sub> layer (Ansmann et al., 2022). Moreover, when the cotton was used several months after the first opening of its package, it is possible that its exposure to atmospheric O<sub>3</sub> (or other oxidants) may have compromised its performance.

635

As reported in the previous paragraph, squalene was confirmed to be an effective and efficient O<sub>3</sub> scrubbing substance, as we expected after consulting existing literature (Coffaro and Weisel, 2022; Coleman et al., 2008; Zhou et al., 2016). Squalene scrubbed O<sub>3</sub> in laboratory tests even down to 250 hPa and around 213 K. Unfortunately, since its testing began after the presented campaigns, squalene-based scrubbers have never been deployed in actual fieldwork.

640

As shown in Figure A2, COS mole fraction was found significantly higher than the bypass channel when O<sub>3</sub> was generated for both with and without the squalene scrubber. This is in contrast with the O<sub>3</sub>-induced COS loss reported in previous studies (Andreae et al., 1990; Engel and Schmidt, 1994; Hofmann et al., 1992; Persson and Leck, 1994). Assuming the glass to be inert, this observation implies that COS is produced either (i) at the UV lamp, likely from traces of VOC or other impurities in the supply gases or (ii) in the tubing downstream of the quartz glass by reactions between O<sub>3</sub> and wall contaminations. When tested on compressed tropospheric air, we could observe the same trends for COS and, although a small decrease was observed for squalene when compared to the bypass channel, it was not statistically significant. We believe the COS enhancement is due to oxidation of other compounds (e.g., CS<sub>2</sub>, DMS) in presence of UV radiation, and not due to the scrubbers themselves. The larger variance for the tests on the scrubbers without O<sub>3</sub> generation is due to some spectroscopical effects that affected the instrument precision during part of the tests (not shown). Either way, no sign of negative biases on COS was measured for either of the two scrubbers.

Overall, it is unclear whether COS may have been simultaneously removed by O<sub>3</sub> and produced by the reaction of O<sub>3</sub> with COS precursors that may have been present as impurities in the air mixture employed for the experiments. This limits the direct comparison with stratospheric field studies (Engel and Schmidt, 1994). Nevertheless, COS mole fraction was significantly lower when ozonated air was measured after passing through the squalene scrubber (or through the cotton scrubber, before saturation) than when it was measured after the control channel. We speculate that new volatile compounds containing carbonyl groups, possibly impurities in the compressed air mixture used for the experiment and/or products of reactions between impurities and O<sub>3</sub>, may have influenced the QCLS spectrum, biasing COS measurements. Different studies report the creation of carbonyl and carboxyl groups on both saturated and unsaturated carbon polymers (Cataldo, 2001; Valls et al., 2022; Zhang et al., 2024; Zhou et al., 2016). However, these reaction products should not contain sulfur compounds. Nevertheless, squalene reduced this bias when compared to the configuration without O<sub>3</sub> scrubbing. Therefore, we believe that most of this bias could have been produced either by products of photochemical reactions due to the UV-lamp employed for O<sub>3</sub> generation, or by reactions of O<sub>3</sub> with impurities or with experimental components. In particular, a phenomenon described as “ozone cracking” is known to affect polymers, such as (vulcanised) rubbers (Cataldo, 2001; Salomon and Van Bloois, 1963; Tse, 2007) and polymers which may be containing sulfur. Therefore, we also speculate that the reaction of O<sub>3</sub> with squalene and its consequent removal may have mitigated these reactions, reducing the production of COS during the performed analyses. Overall, there is no indication that squalene would negatively bias COS measurements, while the presence of O<sub>3</sub> could be detrimental for the measurements, in particular when in presence of unsaturated polymers, which may be prone to degradation. Unfortunately, the effect of O<sub>3</sub> on long-term stored samples was not investigated within this study.

### **Data availability**

The data used in this work are available from <https://doi.org/10.5281/zenodo.15749915> (Zanchetta et al., 2025).

675 **Author contribution**

HC and MK conceived the concept, SvH, AZ and HC designed the experiment, AZ, SvH, JH, RK, TL, MR, ML, PN, SLB, and HC collected the data. AZ, SvH, and HC wrote the manuscript with contribution from all authors.

**Competing interests**

680 Huilin Chen is a member of the editorial board of Atmospheric Measurement Techniques.

**Acknowledgements**

We are grateful for the support during the preparation of the campaigns by Bert Kers, Marcel de Vries and Marc Bleeker at the Center of Isotope Research. We would like to thank the colleagues who collaborated during the campaigns, especially  
685 Maria Elena Popa, Johannes Laube and Johannes Degen. We thank Gisele Krysztofiak and Valery Catoire (LPC2E) for providing their in situ balloon-borne SPIRALE spectrometer observations made in 2009 and 2011. The dataset is maintained by the French national centre for Atmospheric data and services AERIS. The AirCore flights were partially supported by the ESA project FRM4GHG.

690 **Financial support**

This research was supported by the ERC advanced funding scheme (AdG 2016 project no. 742798, project abbreviation COS-OCS), and by the Ruisdael Observatory infrastructure cofinanced by the Dutch Research Council (NWO, Grant No. 184.034.015) and ICOS Netherlands. This work was also supported by the Natural Science Foundation of China (42475115) and by the Fundamental Research Funds for the Central Universities (14380235).

695 **References**

- Andreae, M. O., Ferek, R. J., Bermond, F., Byrd, K. P., Engstrom, R. T., Hardin, S., Houmère, P. D., LeMarrec, F., Raemdonck, H., and Chatfield, R. B.: Dimethyl sulfide in the marine atmosphere, *J. Geophys. Res. Atmospheres*, 90, 12891–12900, <https://doi.org/10.1029/JD090iD07p12891>, 1985.
- Andreae, T. W., Andreae, M. O., Bingemer, H. G., and Leck, C.: Measurements of DMS and H<sub>2</sub>S over the western north atlantic and the tropical atlantic, in *AGU Abstracts (Fall Meeting, 1990)*, *Eos Trans. Am. Geophys. Union*, 71, 1219–1750, <https://doi.org/10.1029/EO071i043p01219>, 1990.
- Andreae, T. W., Andreae, M. O., Bingemer, H. G., and Leck, C.: Measurements of dimethyl sulfide and H<sub>2</sub>S over the western North Atlantic and the tropical Atlantic, *J. Geophys. Res. Atmospheres*, 98, 23389–23396, <https://doi.org/10.1029/91JD03016>, 1993.
- 705 Ansmann, A., Ohneiser, K., Chudnovsky, A., Knopf, D. A., Eloranta, E. W., Villanueva, D., Seifert, P., Radenz, M., Barja, B., Zamorano, F., Jimenez, C., Engelmann, R., Baars, H., Griesche, H., Hofer, J.,

- Althausen, D., and Wandinger, U.: Ozone depletion in the Arctic and Antarctic stratosphere induced by wildfire smoke, *Atmospheric Chem. Phys.*, 22, 11701–11726, <https://doi.org/10.5194/acp-22-11701-2022>, 2022.
- 710 Barkley, M. P., Palmer, P. I., Boone, C. D., Bernath, P. F., and Suntharalingam, P.: Global distributions of carbonyl sulfide in the upper troposphere and stratosphere, *Geophys. Res. Lett.*, 35, L14810, <https://doi.org/10.1029/2008GL034270>, 2008.
- Belviso, S., Remaud, M., Abadie, C., Maignan, F., Ramonet, M., and Peylin, P.: Ongoing Decline in the Atmospheric COS Seasonal Cycle Amplitude over Western Europe: Implications for Surface Fluxes, *Atmosphere*, 13, 812, <https://doi.org/10.3390/atmos13050812>, 2022.
- 715 Bernath, P. F.: Atmospheric Chemistry Experiment (ACE): Mission overview, *Geophys. Res. Lett.*, 32, L15S01, <https://doi.org/10.1029/2005GL022386>, 2005.
- Bernath, P. F., Steffen, J., Crouse, J., and Boone, C. D.: Sixteen-year trends in atmospheric trace gases from orbit, *J. Quant. Spectrosc. Radiat. Transf.*, 253, 107178, <https://doi.org/10.1016/j.jqsrt.2020.107178>, 2020.
- 720 Bernhard, G. H., Bais, A. F., Aucamp, P. J., Klekociuk, A. R., Liley, J. B., and McKenzie, R. L.: Stratospheric ozone, UV radiation, and climate interactions, *Photochem. Photobiol. Sci.*, 22, 937–989, <https://doi.org/10.1007/s43630-023-00371-y>, 2023.
- Berry, J., Wolf, A., Campbell, J. E., Baker, I., Blake, N., Blake, D., Denning, A. S., Kawa, S. R., Montzka, S. A., Seibt, U., Stimler, K., Yakir, D., and Zhu, Z.: A coupled model of the global cycles of carbonyl sulfide and CO<sub>2</sub>: A possible new window on the carbon cycle, *J. Geophys. Res. Biogeosciences*, 118, 842–852, <https://doi.org/10.1002/jgrg.20068>, 2013.
- 725 Boone, C. D., Bernath, P. F., and Lecours, M.: Version 5 retrievals for ACE-FTS and ACE-imagers, *J. Quant. Spectrosc. Radiat. Transf.*, 310, 108749, <https://doi.org/10.1016/j.jqsrt.2023.108749>, 2023.
- 730 Brühl, C., Lelieveld, J., Crutzen, P. J., and Tost, H.: The role of carbonyl sulphide as a source of stratospheric sulphate aerosol and its impact on climate, *Atmospheric Chem. Phys.*, 12, 1239–1253, <https://doi.org/10.5194/acp-12-1239-2012>, 2012.
- Cadle, S. H. and Williams, R. L.: Gas and Particle Emissions from Automobile Tires in Laboratory and Field Studies, *J. Air Pollut. Control Assoc.*, 28, 502–507, <https://doi.org/10.1080/00022470.1978.10470623>, 1978.
- 735 Campbell, J. E., Carmichael, G. R., Chai, T., Mena-Carrasco, M., Tang, Y., Blake, D. R., Blake, N. J., Vay, S. A., Collatz, G. J., Baker, I., Berry, J. A., Montzka, S. A., Sweeney, C., Schnoor, J. L., and Stanier, C. O.: Photosynthetic Control of Atmospheric Carbonyl Sulfide During the Growing Season, *Science*, 322, 1085–1088, <https://doi.org/10.1126/science.1164015>, 2008.

- 740 Cataldo, F.: On the ozone protection of polymers having non-conjugated unsaturation, *Polym. Degrad. Stab.*, 72, 287–296, [https://doi.org/10.1016/S0141-3910\(01\)00017-9](https://doi.org/10.1016/S0141-3910(01)00017-9), 2001.
- Chin, M. and Davis, D. D.: A reanalysis of carbonyl sulfide as a source of stratospheric background sulfur aerosol, *J. Geophys. Res. Atmospheres*, 100, 8993–9005, <https://doi.org/10.1029/95JD00275>, 1995.
- 745 Coffaro, B. and Weisel, C. P.: Reactions and Products of Squalene and Ozone: A Review, *Environ. Sci. Technol.*, 56, 7396–7411, <https://doi.org/10.1021/acs.est.1c07611>, 2022.
- Coffey, M. T. and Hannigan, J. W.: The temporal trend of stratospheric carbonyl sulfide, *J. Atmospheric Chem.*, 67, 61–70, <https://doi.org/10.1007/s10874-011-9203-4>, 2010.
- 750 Coleman, B. K., Destailats, H., Hodgson, A. T., and Nazaroff, W. W.: Ozone consumption and volatile byproduct formation from surface reactions with aircraft cabin materials and clothing fabrics, *Atmos. Environ.*, 42, 642–654, <https://doi.org/10.1016/j.atmosenv.2007.10.001>, 2008.
- Crutzen, P. J.: The possible importance of CSO for the sulfate layer of the stratosphere, *Geophys. Res. Lett.*, 3, 73–76, <https://doi.org/10.1029/GL003i002p00073>, 1976.
- 755 Dirksen, R. J., Boersma, K. F., Eskes, H. J., Ionov, D. V., Bucsela, E. J., Levelt, P. F., and Kelder, H. M.: Evaluation of stratospheric NO<sub>2</sub> retrieved from the Ozone Monitoring Instrument: Intercomparison, diurnal cycle, and trending, *J. Geophys. Res.*, 116, D08305, <https://doi.org/10.1029/2010JD014943>, 2011.
- Engel, A. and Schmidt, U.: Vertical profile measurements of carbonylsulfide in the stratosphere, *Geophys. Res. Lett.*, 21, 2219–2222, <https://doi.org/10.1029/94GL01461>, 1994.
- 760 Ferm, R. J.: The Chemistry Of Carbonyl Sulfide, *Chem. Rev.*, 57, 621–640, <https://doi.org/10.1021/cr50016a002>, 1957.
- Frith, S. M., Bhartia, P. K., Oman, L. D., Kramarova, N. A., McPeters, R. D., and Labow, G. J.: Model-based climatology of diurnal variability in stratospheric ozone as a data analysis tool, *Atmospheric Meas. Tech.*, 13, 2733–2749, <https://doi.org/10.5194/amt-13-2733-2020>, 2020.
- 765 Glatthor, N., Höpfner, M., Leyser, A., Stiller, G. P., Von Clarmann, T., Grabowski, U., Kellmann, S., Linden, A., Sinnhuber, B.-M., Kryzstofiak, G., and Walker, K. A.: Global carbonyl sulfide (OCS) measured by MIPAS/Envisat during 2002–2012, *Atmospheric Chem. Phys.*, 17, 2631–2652, <https://doi.org/10.5194/acp-17-2631-2017>, 2017.
- 770 Gurganus, C., Rollins, A. W., Waxman, E., Pan, L. L., Smith, W. P., Rei Ueyama, Feng, W., Chipperfield, M. P., Atlas, E. L., Schwarz, J. P., Lee, S., and Thornberry, T. D.: Highlighting the impact

of anthropogenic OCS emissions on the stratospheric sulfur budget with in-situ observations, *Authorea* Authorea, <https://doi.org/10.22541/essoar.172801406.62154439/v1>, 2024.

- 775 Hannigan, J. W., Ortega, I., Shams, S. B., Blumenstock, T., Campbell, J. E., Conway, S., Flood, V., Garcia, O., Griffith, D., Grutter, M., Hase, F., Jeseck, P., Jones, N., Mahieu, E., Makarova, M., De Mazière, M., Morino, I., Murata, I., Nagahama, T., Nakijima, H., Notholt, J., Palm, M., Poberovskii, A., Rettinger, M., Robinson, J., Röhring, A. N., Schneider, M., Servais, C., Smale, D., Stremme, W., Strong, K., Sussmann, R., Te, Y., Vigouroux, C., and Wizenberg, T.: Global Atmospheric OCS Trend Analysis From 22 NDACC Stations, *J. Geophys. Res. Atmospheres*, 127, e2021JD035764, <https://doi.org/10.1029/2021JD035764>, 2022.
- 780 Hofmann, U., Hofmann, R., and Kesselmeier, J.: Cryogenic trapping of reduced sulfur compounds using a nafion drier and cotton wadding as an oxidant scavenger, *Atmospheric Environ. Part Gen. Top.*, 26, 2445–2449, [https://doi.org/10.1016/0960-1686\(92\)90374-T](https://doi.org/10.1016/0960-1686(92)90374-T), 1992.
- 785 Hooghiem, J. J. D., de Vries, M., Been, H. A., Heikkinen, P., Kivi, R., and Chen, H.: LISA: a lightweight stratospheric air sampler, *Atmospheric Meas. Tech.*, 11, 6785–6801, <https://doi.org/10.5194/amt-11-6785-2018>, 2018.
- Karion, A., Sweeney, C., Tans, P., and Newberger, T.: AirCore: An Innovative Atmospheric Sampling System, *J. Atmospheric Ocean. Technol.*, 27, 1839–1853, <https://doi.org/10.1175/2010JTECHA1448.1>, 2010.
- 790 Karu, E., Li, M., Ernle, L., Brenninkmeijer, C. A. M., Lelieveld, J., and Williams, J.: Carbonyl Sulfide (OCS) in the Upper Troposphere/Lowermost Stratosphere (UT/LMS) Region: Estimates of Lifetimes and Fluxes, *Geophys. Res. Lett.*, 50, e2023GL105826, <https://doi.org/10.1029/2023GL105826>, 2023.
- Kivi, R. and Heikkinen, P.: Fourier transform spectrometer measurements of column CO<sub>2</sub> at Sodankylä, Finland, *Geosci. Instrum. Methods Data Syst.*, 5, 271–279, <https://doi.org/10.5194/gi-5-271-2016>, 2016.
- 795 Kloss, C., Tan, V., Leen, J. B., Madsen, G. L., Gardner, A., Du, X., Kulesa, T., Schillings, J., Schneider, H., Schrade, S., Qiu, C., and Von Hobe, M.: Airborne Mid-Infrared Cavity enhanced Absorption spectrometer (AMICA), *Atmospheric Meas. Tech.*, 14, 5271–5297, <https://doi.org/10.5194/amt-14-5271-2021>, 2021.
- 800 Kondo, Y., Schmidt, U., Sugita, T., Engel, A., Koike, M., Aïmedieu, P., Gunson, M. R., and Rodriguez, J.: NO<sub>y</sub> correlation with N<sub>2</sub>O and CH<sub>4</sub> in the midlatitude stratosphere, *Geophys. Res. Lett.*, 23, 2369–2372, <https://doi.org/10.1029/96GL00870>, 1996.
- Kooijmans, L. M. J., Uitslag, N. A. M., Zahniser, M. S., Nelson, D. D., Montzka, S. A., and Chen, H.: Continuous and high-precision atmospheric concentration measurements of COS, CO<sub>2</sub>, CO and H<sub>2</sub>O using a quantum cascade laser spectrometer (QCLS), *Atmospheric Meas. Tech.*, 9, 5293–5314, <https://doi.org/10.5194/amt-9-5293-2016>, 2016.

- 805 Kremser, S., Jones, N. B., Palm, M., Lejeune, B., Wang, Y., Smale, D., and Deutscher, N. M.: Positive trends in Southern Hemisphere carbonyl sulfide, *Geophys. Res. Lett.*, 42, 9473–9480, <https://doi.org/10.1002/2015GL065879>, 2015.
- Kremser, S., Thomason, L. W., von Hobe, M., Hermann, M., Deshler, T., Timmreck, C., Toohey, M., Stenke, A., Schwarz, J. P., Weigel, R., Fueglistaler, S., Prata, F. J., Vernier, J.-P., Schlager, H., Barnes, J. E., Antuña-Marrero, J.-C., Fairlie, D., Palm, M., Mahieu, E., Notholt, J., Rex, M., Bingen, C., Vanhellemont, F., Bourassa, A., Plane, J. M. C., Klocke, D., Carn, S. A., Clarisse, L., Trickl, T., Neely, R., James, A. D., Rieger, L., Wilson, J. C., and Meland, B.: Stratospheric aerosol-Observations, processes, and impact on climate: Stratospheric Aerosol, *Rev. Geophys.*, 54, 278–335, <https://doi.org/10.1002/2015RG000511>, 2016.
- 810
- 815 Krysztofiak, G., Té, Y. V., Catoire, V., Berthet, G., Toon, G. C., Jégou, F., Jeseck, P., and Robert, C.: Carbonyl Sulphide (OCS) Variability with Latitude in the Atmosphere, *Atmosphere-Ocean*, 53, 89–101, <https://doi.org/10.1080/07055900.2013.876609>, 2015.
- Laube, J. C., Engel, A., Bönisch, H., Möbius, T., Sturges, W. T., Braß, M., and Röckmann, T.: Fractional release factors of long-lived halogenated organic compounds in the tropical stratosphere, *Atmospheric Chem. Phys.*, 10, 1093–1103, <https://doi.org/10.5194/acp-10-1093-2010>, 2010.
- 820
- Lee, C.-L. and Brimblecombe, P.: Anthropogenic contributions to global carbonyl sulfide, carbon disulfide and organosulfides fluxes, *Earth-Sci. Rev.*, 160, 1–18, <https://doi.org/10.1016/j.earscirev.2016.06.005>, 2016.
- Lejeune, B., Mahieu, E., Vollmer, M. K., Reimann, S., Bernath, P. F., Boone, C. D., Walker, K. A., and Servais, C.: Optimized approach to retrieve information on atmospheric carbonyl sulfide (OCS) above the Jungfraujoch station and change in its abundance since 1995, *J. Quant. Spectrosc. Radiat. Transf.*, 186, 81–95, <https://doi.org/10.1016/j.jqsrt.2016.06.001>, 2017.
- 825
- Leung, F. T., Colussi, A. J., Hoffmann, M. R., and Toon, G. C.: Isotopic fractionation of carbonyl sulfide in the atmosphere: Implications for the source of background stratospheric sulfate aerosol, *Geophys. Res. Lett.*, 29, <https://doi.org/10.1029/2001GL013955>, 2002.
- 830
- Levine, Y., Chetrit, E., Fishman, Y., Siyum, Y., Rabaev, M., Fletcher, A., and Tartakovsky, K.: A novel approach to plasticizer content calculation in an acrylonitrile-butadiene rubber real-time aging study (NBR), *Polym. Test.*, 124, 108091, <https://doi.org/10.1016/j.polymertesting.2023.108091>, 2023.
- Li, K.-F., Khoury, R., Pongetti, T. J., Sander, S. P., Mills, F. P., and Yung, Y. L.: Diurnal variability of stratospheric column NO<sub>2</sub> measured using direct solar and lunar spectra over Table Mountain, California (34.38° N), *Atmospheric Meas. Tech.*, 14, 7495–7510, <https://doi.org/10.5194/amt-14-7495-2021>, 2021.
- 835

- 840 Ma, J., Kooijmans, L. M. J., Cho, A., Montzka, S. A., Glatthor, N., Worden, J. R., Kuai, L., Atlas, E. L.,  
and Krol, M. C.: Inverse modelling of carbonyl sulfide: implementation, evaluation and implications for  
the global budget, *Atmospheric Chem. Phys.*, 21, 3507–3529, [https://doi.org/10.5194/acp-21-3507-](https://doi.org/10.5194/acp-21-3507-2021)  
2021, 2021.
- 845 Membrive, O., Crevoisier, C., Sweeney, C., Danis, F., Hertzog, A., Engel, A., Bönisch, H., and Picon,  
L.: AirCore-HR: a high-resolution column sampling to enhance the vertical description of  
 $\text{CH}_4$  and  $\text{CO}_2$ , *Atmospheric Meas. Tech.*, 10, 2163–  
2181, <https://doi.org/10.5194/amt-10-2163-2017>, 2017.
- Montzka, S. A., Calvert, P., Hall, B. D., Elkins, J. W., Conway, T. J., Tans, P. P., and Sweeney, C.: On  
the global distribution, seasonality, and budget of atmospheric carbonyl sulfide (COS) and some  
similarities to  $\text{CO}_2$ , *J. Geophys. Res.*, 112, D09302, <https://doi.org/10.1029/2006JD007665>, 2007.
- 850 Persson, Cecilia. and Leck, Caroline.: Determination of Reduced Sulfur Compounds in the Atmosphere  
Using a Cotton Scrubber for Oxidant Removal and Gas Chromatography with Flame Photometric  
Detection, *Anal. Chem.*, 66, 983–987, <https://doi.org/10.1021/ac00079a009>, 1994.
- Picardo, M., Ottaviani, M., Camera, E., and Mastrofrancesco, A.: Sebaceous gland lipids,  
*Dermatoendocrinol.*, 1, 68–71, <https://doi.org/10.4161/derm.1.2.8472>, 2009.
- 855 Plumb, R. A.: Tracer interrelationships in the stratosphere, *Rev. Geophys.*, 45,  
<https://doi.org/10.1029/2005RG000179>, 2007.
- Plumb, R. A. and Ko, M. K. W.: Interrelationships between mixing ratios of long-lived stratospheric  
constituents, *J. Geophys. Res. Atmospheres*, 97, 10145–10156, <https://doi.org/10.1029/92JD00450>,  
1992.
- 860 Pos, W. H. and Berresheim, H.: Automotive tire wear as a source for atmospheric OCS and  $\text{CS}_2$ ,  
*Geophys. Res. Lett.*, 20, 815–817, <https://doi.org/10.1029/93GL00972>, 1993.
- 865 Remaud, M., Ma, J., Krol, M., Abadie, C., Cartwright, M. P., Patra, P., Niwa, Y., Rodenbeck, C.,  
Belviso, S., Kooijmans, L., Lennartz, S., Maignan, F., Chevallier, F., Chipperfield, M. P., Pope, R. J.,  
Harrison, J. J., Vimont, I., Wilson, C., and Peylin, P.: Intercomparison of Atmospheric Carbonyl Sulfide  
(TransCom-COS; Part One): Evaluating the Impact of Transport and Emissions on Tropospheric  
Variability Using Ground-Based and Aircraft Data, *J. Geophys. Res. Atmospheres*, 128,  
[e2022JD037817](https://doi.org/10.1029/2022JD037817), <https://doi.org/10.1029/2022JD037817>, 2023.
- Rinsland, C. P., Chiou, L., Mahieu, E., Zander, R., Boone, C. D., and Bernath, P. F.: Measurements of  
long-term changes in atmospheric OCS (carbonyl sulfide) from infrared solar observations, *J. Quant.  
Spectrosc. Radiat. Transf.*, 109, 2679–2686, <https://doi.org/10.1016/j.jqsrt.2008.07.008>, 2008.

- 870 Salomon, G. and Van Bloois, F.: The mechanism of ozone cracking. I. Ozone cracking of plastic films, *J. Appl. Polym. Sci.*, 7, 1117–1132, <https://doi.org/10.1002/app.1963.070070325>, 1963.
- Sandoval-Soto, L., Stanimirov, M., Von Hobe, M., Schmitt, V., Valdes, J., Wild, A., and Kesselmeier, J.: Global uptake of carbonyl sulfide (COS) by terrestrial vegetation: Estimates corrected by deposition velocities normalized to the uptake of carbon dioxide (CO<sub>2</sub>), *Biogeosciences*, 2, 125–132, 875 <https://doi.org/10.5194/bg-2-125-2005>, 2005.
- Schmidt, M., Bernath, P., Boone, C., Lecours, M., and Steffen, J.: Trends in atmospheric composition between 2004–2023 using version 5 ACE-FTS data, *J. Quant. Spectrosc. Radiat. Transf.*, 325, 109088, <https://doi.org/10.1016/j.jqsrt.2024.109088>, 2024.
- Schmidt, U., Kulesa, G., Klein, E., Röth, E.-P., Fabian, P., and Borchers, R.: Intercomparison of 880 balloon-borne cryogenic whole air samplers during the MAP/GLOBUS 1983 campaign, *Planet. Space Sci.*, 35, 647–656, [https://doi.org/10.1016/0032-0633\(87\)90131-0](https://doi.org/10.1016/0032-0633(87)90131-0), 1987.
- Schranz, F., Fernandez, S., Kämpfer, N., and Palm, M.: Diurnal variation in middle-atmospheric ozone observed by ground-based microwave radiometry at Ny-Ålesund over 1 year, *Atmospheric Chem. Phys.*, 18, 4113–4130, <https://doi.org/10.5194/acp-18-4113-2018>, 2018.
- 885 Schuck, T. J., Degen, J., Keber, T., Meixner, K., Wagenhäuser, T., Ghysels, M., Durry, G., Amarouche, N., Zanchetta, A., Van Heuven, S., Chen, H., Laube, J. C., Baartman, S. L., Van Der Veen, C., Popa, M. E., and Engel, A.: Measurement report: Greenhouse gas profiles and age of air from the 2021 HEMERA-TWIN balloon launch, *Atmospheric Chem. Phys.*, 25, 4333–4348, <https://doi.org/10.5194/acp-25-4333-2025>, 2025.
- 890 Supel™-Inert Multi-Layer Foil: <https://www.sigmaldrich.com/NL/en/product/supelco/30228u>, last access: 30 April 2025.
- Stimler, K., Nelson, D., and Yakir, D.: High precision measurements of atmospheric concentrations and plant exchange rates of carbonyl sulfide using mid-IR quantum cascade laser, *Glob. Change Biol.*, <https://doi.org/10.1111/j.1365-2486.2009.02088.x>, 2009.
- 895 Studer, S., Hocke, K., Schanz, A., Schmidt, H., and Kämpfer, N.: A climatology of the diurnal variations in stratospheric and mesospheric ozone over Bern, Switzerland, *Atmospheric Chem. Phys.*, 14, 5905–5919, <https://doi.org/10.5194/acp-14-5905-2014>, 2014.
- Sturges, W. T., Penkett, S. A., Barnola, J., Chappellaz, J., Atlas, E., and Stroud, V.: A long-term record of carbonyl sulfide (COS) in two hemispheres from firn air measurements, *Geophys. Res. Lett.*, 28, 900 4095–4098, <https://doi.org/10.1029/2001GL013958>, 2001.
- Tans, P.: Fill dynamics and sample mixing in the AirCore, *Atmospheric Meas. Tech.*, 15, 1903–1916, <https://doi.org/10.5194/amt-15-1903-2022>, 2022.

- 905 Tong, X., Van Heuven, S., Scheeren, B., Kers, B., Hutjes, R., and Chen, H.: Aircraft-Based AirCore Sampling for Estimates of N<sub>2</sub>O and CH<sub>4</sub> Emissions, *Environ. Sci. Technol.*, 57, 15571–15579, <https://doi.org/10.1021/acs.est.3c04932>, 2023.
- Toon, G. C., Blavier, J.-F. L., and Sung, K.: Atmospheric carbonyl sulfide (OCS) measured remotely by FTIR solar absorption spectrometry, *Atmospheric Chem. Phys.*, 18, 1923–1944, <https://doi.org/10.5194/acp-18-1923-2018>, 2018.
- 910 Tse, M. F.: Ozone cracking and flex cracking of crosslinked polymer blend compounds, *J. Appl. Polym. Sci.*, 103, 2183–2196, <https://doi.org/10.1002/app.25139>, 2007.
- Valls, C., Cusola, O., and Roncero, M. B.: Evaluating the potential of ozone in creating functional groups on cellulose, *Cellulose*, 29, 6595–6610, <https://doi.org/10.1007/s10570-022-04694-4>, 2022.
- 915 Velazco, V. A., Toon, G. C., Blavier, J.-F. L., Kleinböhl, A., Manney, G. L., Daffer, W. H., Bernath, P. F., Walker, K. A., and Boone, C.: Validation of the Atmospheric Chemistry Experiment by noncoincident MkIV balloon profiles, *J. Geophys. Res.*, 116, D06306, <https://doi.org/10.1029/2010JD014928>, 2011.
- Vinković, K., Andersen, T., De Vries, M., Kers, B., Van Heuven, S., Peters, W., Hensen, A., Van Den Bulk, P., and Chen, H.: Evaluating the use of an Unmanned Aerial Vehicle (UAV)-based active AirCore system to quantify methane emissions from dairy cows, *Sci. Total Environ.*, 831, 154898, <https://doi.org/10.1016/j.scitotenv.2022.154898>, 2022.
- 920 Wagenhäuser, T., Engel, A., and Sitals, R.: Testing the altitude attribution and vertical resolution of AirCore measurements with a new spiking method, *Atmospheric Meas. Tech.*, 14, 3923–3934, <https://doi.org/10.5194/amt-14-3923-2021>, 2021.
- 925 Whelan, M. E., Lennartz, S. T., Gimeno, T. E., Wehr, R., Wohlfahrt, G., Wang, Y., Kooijmans, L. M. J., Hilton, T. W., Belviso, S., Peylin, P., Commane, R., Sun, W., Chen, H., Kuai, L., Mammarella, I., Maseyk, K., Berkelhammer, M., Li, K.-F., Yakir, D., Zumkehr, A., Katayama, Y., Ogée, J., Spielmann, F. M., Kitz, F., Rastogi, B., Kesselmeier, J., Marshall, J., Erkkilä, K.-M., Wingate, L., Meredith, L. K., He, W., Bunk, R., Launois, T., Vesala, T., Schmidt, J. A., Fichot, C. G., Seibt, U., Saleska, S., Saltzman, E. S., Montzka, S. A., Berry, J. A., and Campbell, J. E.: Reviews and syntheses: Carbonyl sulfide as a multi-scale tracer for carbon and water cycles, *Biogeosciences*, 15, 3625–3657, <https://doi.org/10.5194/bg-15-3625-2018>, 2018.
- 930 Wofsy, S., Daube, B., Jimenez-Pizarro, R., Kort, E., Pittman, J., Park, S., Commane, R., Xiang, B., Santoni, G., Jacob, D., Fisher, J., Pickett-Heaps, C., Wang, H., Wecht, K., Wang, Q., Stephens, B., Shertz, S., Watt, A., Romashkin, P., Campos, T., Haggerty, J., Cooper, W., Rogers, D., Beaton, S., Hendershot, R., Elkins, J., Fahey, D., Gao, R., Schwarz, J., Moore, F., Montzka, S., Perring, A., Hurst, D., Miller, B., Sweeney, C., Oltmans, S., Hintsä, E., Nance, D., Dutton, G., Watts, L., Spackman, J., Rosenlof, K., Ray, E., Hall, B., Zondlo, M., Diao, M., Keeling, R., Bent, J., Atlas, E., Lueb, R., and M.

J. Mahoney (Deceased): HIPPO Combined Discrete Flask and GC Sample GHG, Halocarbon, and Hydrocarbon Data. Version 1.0 (1.0), [https://doi.org/10.3334/CDIAC/HIPPO\\_012](https://doi.org/10.3334/CDIAC/HIPPO_012), 2017.

940 Wofsy, S. C.: HIAPER Pole-to-Pole Observations (HIPPO): fine-grained, global-scale measurements of climatically important atmospheric gases and aerosols, *Philos. Trans. R. Soc. Math. Phys. Eng. Sci.*, 369, 2073–2086, <https://doi.org/10.1098/rsta.2010.0313>, 2011.

World Meteorological Organization (WMO): *Meteorology – A three-dimensional science: Second session of the Commission for Aerology*, 1957.

945 World Meteorological Organization (WMO): *Scientific assessment of ozone depletion, 1998*, edited by: National Oceanic and Atmospheric Administration, National Aeronautics and Space Administration, United Nations Environment Programme, World Meteorological Organization, and European Commission, National Oceanic and Atmospheric Administration : National Aeronautics and Space Administration ; United Nations Environment Programme ; World Meteorological Organization ; European Commission, Washington, DC : Nairobi, Kenya : Geneva, Switzerland : Brussels, Belgium, 1  
950 pp., 1999.

Yousefi, M., Bernath, P. F., Boone, C. D., and Toon, G. C.: Global measurements of atmospheric carbonyl sulfide (OCS), OC34S and O13CS, *J. Quant. Spectrosc. Radiat. Transf.*, 238, 106554, <https://doi.org/10.1016/j.jqsrt.2019.06.033>, 2019.

955 Zanchetta, A., Kooijmans, L. M. J., Van Heuven, S., Scifo, A., Scheeren, H. A., Mammarella, I., Karstens, U., Ma, J., Krol, M., and Chen, H.: Sources and sinks of carbonyl sulfide inferred from tower and mobile atmospheric observations in the Netherlands, *Biogeosciences*, 20, 3539–3553, <https://doi.org/10.5194/bg-20-3539-2023>, 2023.

960 Zhang, L., Fu, J., Gao, W., Li, Y., and Fan, X.: Revealing the structural variation and degradation mechanism of cellulose during ozone oxidation treatment, *Ind. Crops Prod.*, 219, 119101, <https://doi.org/10.1016/j.indcrop.2024.119101>, 2024.

Zhou, S., Forbes, M. W., Katrib, Y., and Abbatt, J. P. D.: Rapid Oxidation of Skin Oil by Ozone, *Environ. Sci. Technol. Lett.*, 3, 170–174, <https://doi.org/10.1021/acs.estlett.6b00086>, 2016.